AD-A193 481 LOW-B ZTB2NG DEVICE FOR HIGH VOLTAGE CONVERTER SAFETY (U) HARRY DIAMOND LABS ADELPHI MD D L OVERMAN ET AL. MAR 88 HDL-TM-88-1

UNCLASSIFIED F/G 19/1 NL

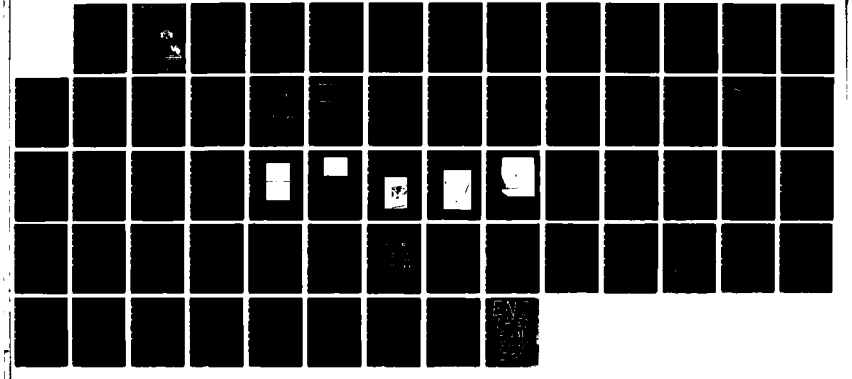

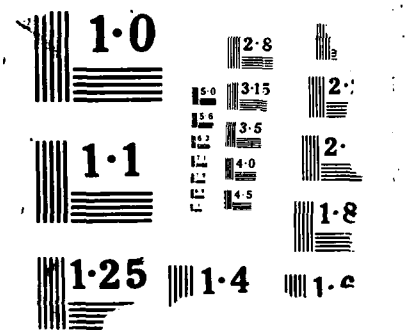
1·0
1·1
1·25
1·4
2·8
3·15
3·5
4·0
4·5
1·8

HDL-TM-88-1

March 1988

Low-G Zigzag Device for High Voltage Converter Safety

by David L. Overman
James L. Beard
Gerd Lohmann
Donald W. Hunter

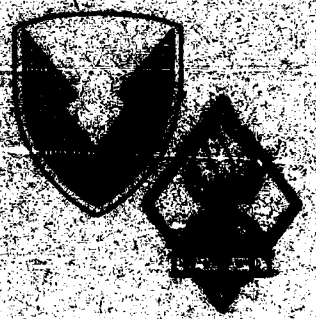

U.S. Army Laboratory Command
Harry Diamond Laboratories
Adelphi, MD 20783-1197

The findings in this report are not to be construed as an official Department of the Army position unless so designated by other authorized documents.

Citation of manufacturers' or trade names does not constitute an official endorsement or approval of the use thereof.

Destroy this report when it is no longer needed. Do not return it to the originator.

UNCLASSIFIED
SECURITY CLASSIFICATION OF THIS PAGE

REPORT DOCUMENTATION PAGE

Form Approved
OMB No 0704-0188
Exp Date Jun 30 1986

1a REPORT SECURITY CLASSIFICATION UNCLASSIFIED	1b RESTRICTIVE MARKINGS
2a SECURITY CLASSIFICATION AUTHORITY	3 DISTRIBUTION / AVAILABILITY OF REPORT Approved for public release; distribution unlimited.
2b DECLASSIFICATION / DOWNGRADING SCHEDULE	
4 PERFORMING ORGANIZATION REPORT NUMBER(S) HDL-TM-88-1	5 MONITORING ORGANIZATION REPORT NUMBER(S)
6a NAME OF PERFORMING ORGANIZATION Harry Diamond Laboratories 6b OFFICE SYMBOL (If applicable) SLCHD-DE-OM	7a NAME OF MONITORING ORGANIZATION
6c ADDRESS (City, State, and ZIP Code) 2800 Powder Mill Road Adelphi, MD 20783-1197	7b ADDRESS (City, State, and ZIP Code)
8a NAME OF FUNDING / SPONSORING ORGANIZATION See reverse. 8b OFFICE SYMBOL (If applicable)	9 PROCUREMENT INSTRUMENT IDENTIFICATION NUMBER
8c ADDRESS (City, State, and ZIP Code) Eglin Air Force Base, FL 32542	10 SOURCE OF FUNDING NUMBERS PROGRAM ELEMENT NO. 62602F; PROJECT NO; TASK NO; WORK UNIT ACCESSION NO

11 TITLE (Include Security Classification)
Low-G Zigzag Device for High Voltage Converter Safety

12 PERSONAL AUTHOR(S)
David L. Overman, James L. Beard, Gerd Lohmann, and Donald W. Hunter

13a TYPE OF REPORT	13b TIME COVERED	14 DATE OF REPORT (Year, Month, Day)	15 PAGE COUNT
Final	FROM Sep 86 TO Jan 87	March 1988	62

16 SUPPLEMENTARY NOTATION
HDL project: 473746

17 COSATI CODES			18 SUBJECT TERMS (Continue on reverse if necessary and identify by block number)
FIELD	GROUP	SUB-GROUP	
16	03		Safety and arming, zigzag device, acceleration sensor, voltage converter, electronic fuzing
19	01		

19 ABSTRACT (Continue on reverse if necessary and identify by block number)

This report describes the design and fabrication of an acceleration sensing mechanism that can be used to provide handling safety in electronic fuzing applications. It compares several different concepts, analyzes the selected concept, defines the model that was built, and presents preliminary test results. The device operates at 9 g to bring together two halves of a magnetic core assembly in a high voltage converter in the arming system. It uses a zigzag cam and flywheel mechanism to achieve a high degree of handling safety, and also has a compact solenoid locking system.

20 DISTRIBUTION / AVAILABILITY OF ABSTRACT	21 ABSTRACT SECURITY CLASSIFICATION
☒ UNCLASSIFIED/UNLIMITED ☐ SAME AS RPT ☐ DTIC USERS	UNCLASSIFIED
22a NAME OF RESPONSIBLE INDIVIDUAL David L. Overman	22b TELEPHONE (Include Area Code) (202) 394-2420 22c OFFICE SYMBOL SLCHD-DE-OM

DD FORM 1473, 84 MAR 83 APR edition may be used until exhausted
All other editions are obsolete

SECURITY CLASSIFICATION OF THIS PAGE
UNCLASSIFIED

8a. NAME OF FUNDING/SPONSORING ORGANIZATION (cont'd)

Air Force Armament and Test Laboratory—AD/DLJ

17. COSATI CODES (cont'd)

FIELD	GROUP
10	02
09	01
	03

Contents

Contents (cont'd)

Figures

1. Introduction

The Air Force Armament and Test Laboratories (AFATL) at Eglin Air Force Base is interested in determining whether it would be feasible to use a zigzag setback device to control the gap in the magnetic core of a high voltage converter in a low-g missile safety mechanism. After some preliminary study and analysis by mechanical systems personnel at Harry Diamond Laboratories (HDL), it was decided that this would be a practical concept to explore. This report summarizes work on the design, analysis, construction, and testing of such a device from October 1986 through January 1987.

2. Background

2.1 Purpose

This device serves as a safety element in an "electronic" safety and arming (S&A) system using slapper detonators. Such an S&A system requires the missile battery voltage to be increased from tens of volts to a level of thousands of volts. A component of the voltage increaser is a step-up converter device using a coil (or coils) of wire and a magnetic core assembly. The converter efficiency can be made extremely dependent on the gap between the halves of the core, as illustrated by figure 1. If the core halves are widely separated, the converter can be ineffective in generating voltages high enough to cause the S&A system's explosive train to function. The zigzag acceleration sensing mechanism can be used to hold the core halves apart and to bring them together if and only if it is driven by the forces from a proper missile launch. Thus, the circuit cannot cause the warhead to function without a proper launch environment.

2.2 Zigzag Device

HDL's previous experience with the development of similar acceleration sensing zigzag safety devices was called on to guide the effort on this project. The zigzag mechanism is composed of a few simple parts, fits in a compact space, and furnishes a high degree of safety in low-g (10 to 1000 g) applications. Safety is provided by a combination of three main features: (1) the product of the overall stroke and spring bias, (2) the

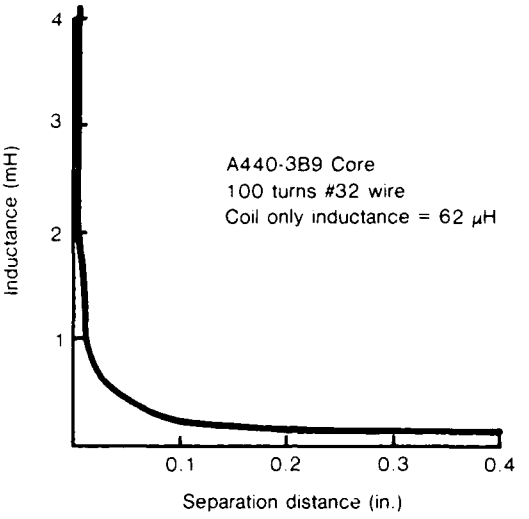

Figure 1. Inductance versus separation for coil and core assembly.

flywheel effect of rotating a large mass with a small moment arm (this applies only to certain configurations considered for this project), and (3) the start and stop action caused by the zigzag track, wherein the mass is forced to rotate in the opposite direction in order to traverse each leg of the track. This third feature is by far the most important. A fourth factor, which can be significant where low-friction bearings are used, is the helix angle. With rolling element bearings, a shallow angle such as 10° can be used to null a large proportion of the drive force into the cam track and thereby increase safety.

2.3 MLRS/M445 Acceleration Lock

The zigzag accceleration lock from the M445/447 electronic time fuzes for the Multiple Launch Rocket System (MLRS) was used as a basis for designing the device for this project (see fig. 2). The MLRS unit uses a 3.35-gram weight, having a radius of gyration of 0.16 in. (driven by a moment arm of 0.08 in.), moving through a linear stroke of 0.6 in. in six 0.1-in.-long by 45° stages. Bias at the start of motion is 10 g and bias at the bottom of the stroke is 14 g. (The M445 fuze specification tests are run at the 20- to 30-g level because the weight must do some work at the bottom of its stroke in that application.) The zigzag cam post from this device is 0.187 in. diam by about 1 in. long and is machined from aluminum. In order to avoid machining a special zigzag cam for this project, the cam from the M445 unit was used with only minor modification of its length.

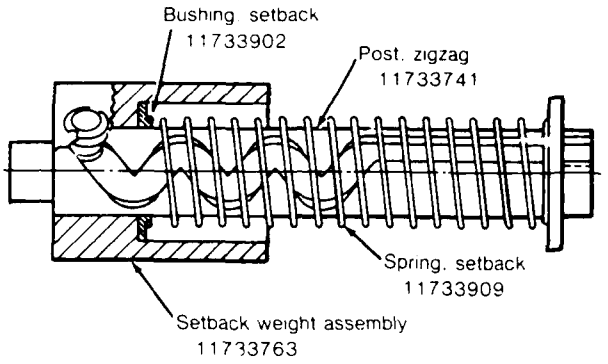

Figure 2. Zigzag acceleration sensor for MLRS/M445 fuze. (numbers on figure are drawing numbers for those parts).

2.4 Safety Analysis

A safety analysis of the MLRS units, resulting in a sensitivity curve for rectangular drive pulses, is shown in figure 3. It shows that the minimum velocity change required to arm this device is 65 ft/s when neglecting the effect of friction. For a friction coefficient of 0.2 the required velocity change is about 17-percent higher. A velocity change of 65 ft/s is equivalent to the speed at the end of a free-fall drop from a height of 65 ft! This minimum delta-V occurs at a drive level of about 25 g. To produce an average drive pulse of 25 g from a 65-ft drop, the unit would have to decelerate at 25 g over a distance of 2.6 ft (equivalent to a 2.6-ft penetration into soft earth). Such a pulse is highly unlikely to result from the usual accidental rough handling situation. And if the drive level is different from 25 g, the graph in figure 3 shows that an even higher velocity change is needed for arming. Thus, it can be seen that such zigzag devices can provide adequate handling safety at bias levels of about 10 g.

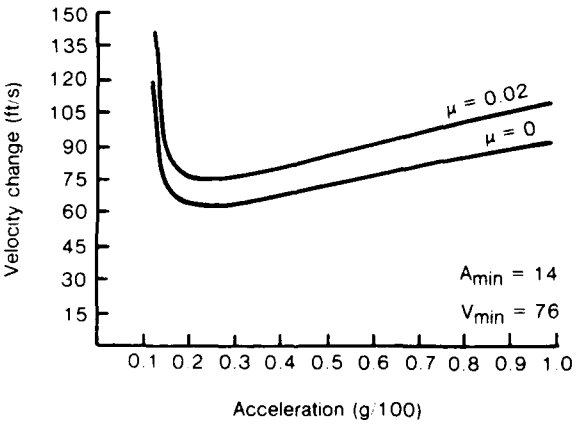

Zigzag design

1. Radius of gyration k = 0.16
2. Radius of interaction r = 0.08
3. Coeff of friction μ = 0.2
4. Number of legs N = 6

Length	angle	lead	mec-con
0.100	45	0.503	7.000
0.100	45	0.503	7.000
0.100	45	0.503	7.000
0.100	45	0.503	7.000
0.100	45	0.503	7.000
0.100	45	0.503	7.000

5. Total stroke of S/M = 0.608
6. Bias at top of stroke = 10g
7. Bias at bottom stroke = 14g

Figure 3. Safety analysis for MLRS/M445 fuze zigzag unit.

3. Project Requirements

The Air Force munition application requires a no-function bias level of 7 g and an all-function level of 11 g. The working levels were selected as 7.5 and 10.5 g. Another requirement was an overall height of less than 1.75 in. and a footprint as small as possible consistent with other design constraints. The project was to emphasize mechanical design rather than electrical. Achieving a compact arrangement, wherein solenoids are used to lock the device in both the safe and the armed conditions, was considered especially important. It was further preferred to use an off-the-shelf magnetic core, small linear solenoids that were on hand, and the existing zigzag cam post as discussed in section 2.2. Theoretical drop safety equivalent to the 65 ft provided by the MLRS device was also deemed appropriate.

4. Design Concepts

Many different design approaches were considered. Some of these are discussed in the following sections.

4.1 Concept A

An initial concept is shown in figure 4. This design is very similar to the MLRS device. It does not include a means for locking the sensing weight in the safe (up) position. Other disadvantages include a bias spring design that would be difficult to implement, poor attachment for the ferrite washer (which would be a nonstandard part), and a lack of positive clamping action from the circumferential groove used to lock the washer to the core at the bottom of the stroke.

4.2 Concept B

The idea here is to place the transformer core in the center of a sensing weight that interfaces with an external zigzag track as illustrated in figure 5. Here, the driving moment arm is much larger than the weight's radius of gyration, so a shallow helix angle and rolling element bearings must be used to obtain adequate drop safety. The concept was analyzed assuming a helix angle of 10°, a carrier radius of gyration of 0.25 (diam about 0.7 in.), a driving moment arm of 0.4 in., a coefficient of friction of 0.05, and

four stages of motion at 0.1 in. each. The resulting minimum safe drop height was about 76 ft for this nominal 9-g device. This concept was not fully developed because, due to the rolling element bearings that would be needed, it was deemed too complex for the quick-response nature of this project. However, it appears promising for future consideration.

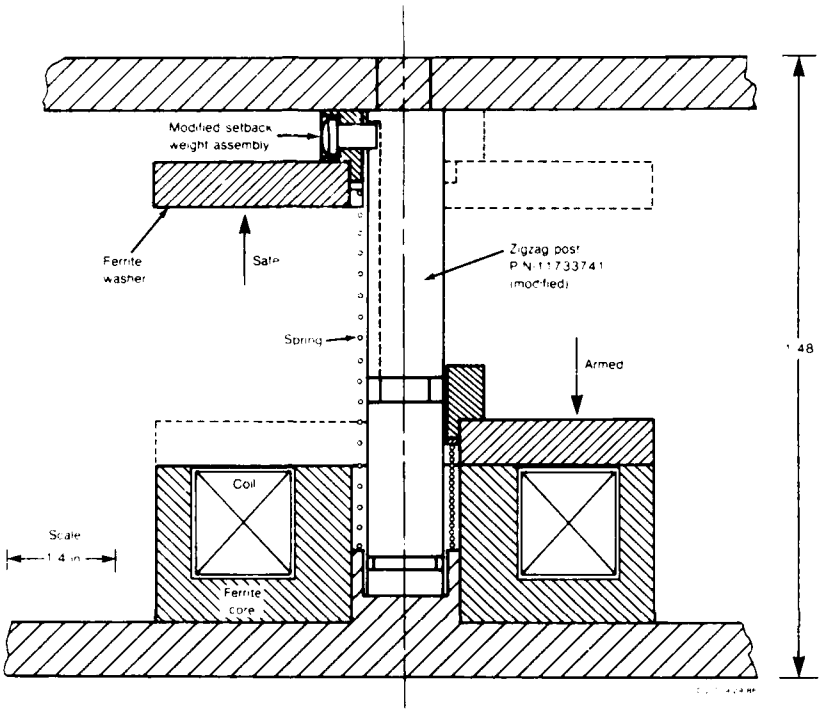

Figure 4. Design concept A.

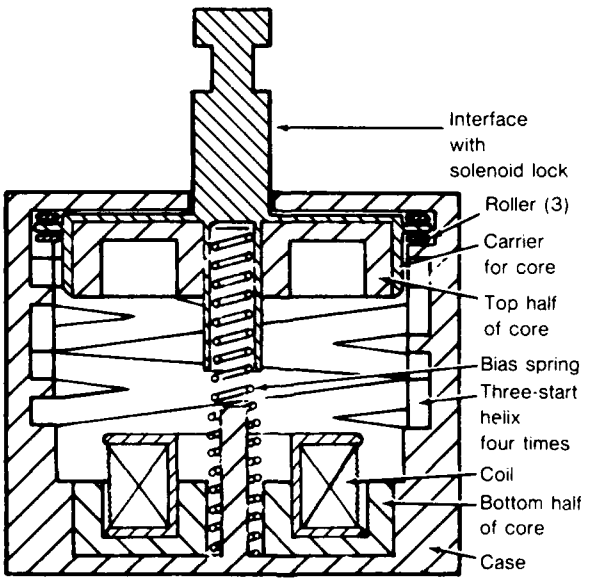

Figure 5. Design concept B.

4.3 Concept C

Figure 6 illustrates a four-stage design using a commercial magnetic core having an outside diameter of 0.9 in. It features a single external bias spring and provides for locking the moveable core element in both the safe and armed positions by a solenoid-actuated half-shaft mechanism as illustrated in figure 7. Also shown in figure 6 is (1) an extension added to lengthen the zigzag cam post of the standard MLRS/M445 fuze's S&A device and (2) a spring washer slip-clutch feature which could be used to prevent the zigzag track from being damaged if the massive, high-inertia weight was driven by a severe overload such as several hundred g's. The spring washer is anchored to the zigzag shaft, and friction between the washer and the top plate is high enough to prevent rotation of the shaft with respect to the plate unless overload conditions are reached. Concept C appeared to be a good workable approach, but it was not considered further because concept D was more compact, more flexible, and easier to implement.

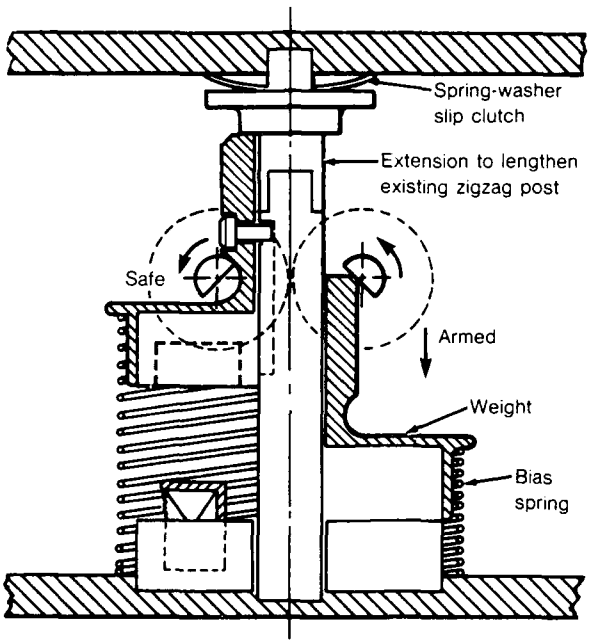

Figure 6. Design concept C.

Figure 7. Unlocking mechanism mounted on back of unit (concept C).

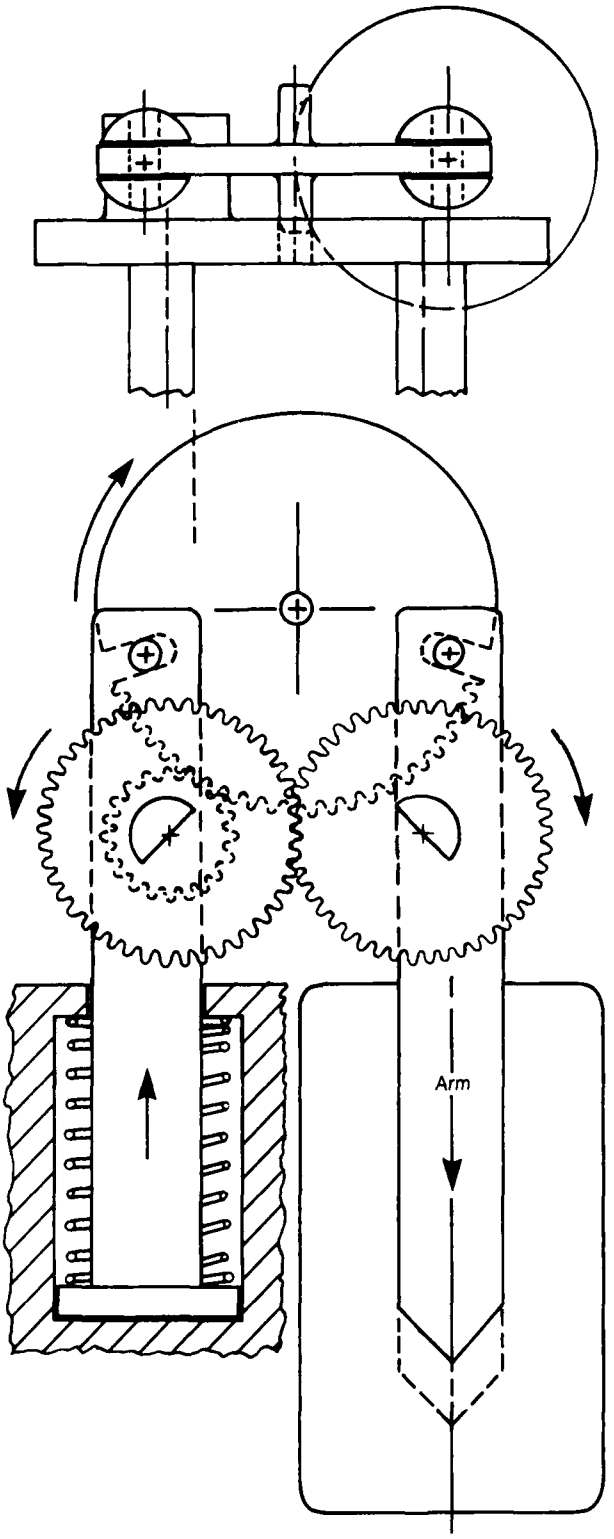

4.4 Concept D

This idea, illustrated in figure 8, is somewhat unconventional in that the sensing weight is constrained to move linearly, and it drives the zigzag cam post with its attached flywheel in an oscillating fashion. The sensing weight is biased by two external springs mounted over the weight's guideposts. The advantages of this concept include a better ability to tailor the spring design to fit the space and force requirements, and the ability to adjust the flywheel properties independent of the sensing weight properties. A solenoid interlock system would sit on top of the unit and engage the flywheel. Since the flywheel is fastened to the zigzag cam post, turning the flywheel can drive the acceleration sensing weight either up or down, depending on the position of the guide pin in the cam track (fig. 8, inset). With the weight in fully up position, torque applied to the flywheel by the solenoid lock forces the weight up toward the safe position. With the weight in the down or armed position, torque applied to the flywheel by the solenoid lock forces the weight (with the top half of the core) down so as to eliminate any air gap between the core halves.

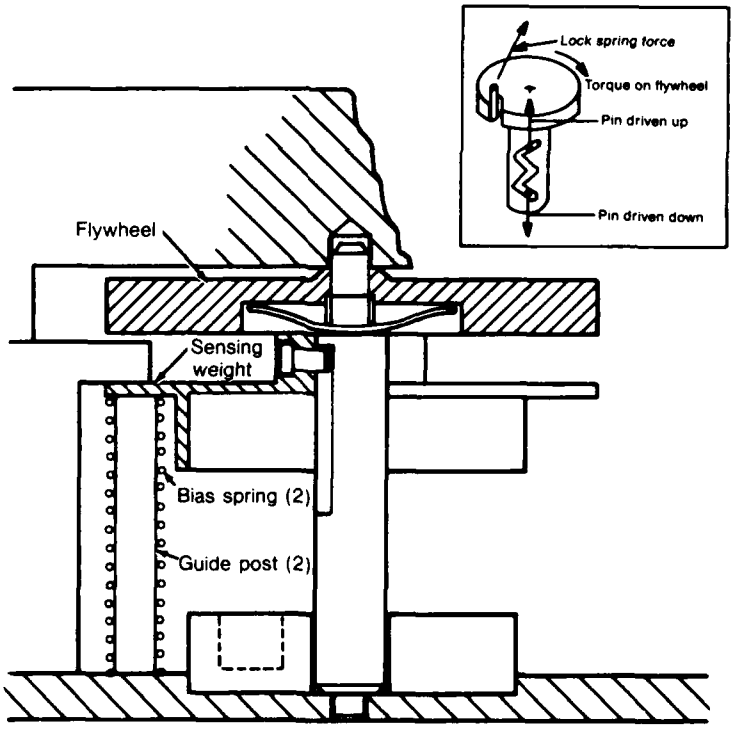

Figure 8. Design concept D.

4.5 Other Concepts

Many different configurations were considered for packaging all the necessary design features in the minimum space. The zigzag safety and transformer elements by themselves are relatively compact. The most difficult problem is to achieve a locking/unlocking and lock-down mechanism that requires a minimum of additional space. A single solenoid to lock the device in both positions is the approach used here. However, electrothermal actuators using bimetals or memory metals such as NITINOL might save additional space. Such actuators could be used in opposed pairs to eliminate the need for shock balancing counterweights as needed when using linear solenoids. Rotary solenoids need no counterweight, but they are not very compact or easy to interface in a small space.

5. Selected Approach

Concept D, presented in figure 8, was selected for implementation as a model. Figure 9 shows various features of the design. The existing zigzag cam post from the M445 fuze S&A device is used by shortening it and machining a pivot on its bottom end. It fits through the center hole in a commercial 0.9-in.-diam magnetic core, as shown in figure 10. The guide pin, which rides in the zigzag track, is mounted in a steel sensing weight that carries the top half of the magnetic core. This weight is guided by two rods around which are two springs designed to provide a minimum 7.5-g bias in the safe (up) position and a maximum 10.5-g bias in the fully armed (down) position. The arrangement allows the weight/core assembly to traverse four equal 0.1-in.-long stages of the zigzag track in going from the safe to the armed position. A steel flywheel (with integral top pivot) measuring 1-in. diam by 0.16 in. thick is fastened to the top of the zigzag cam post. A 0.50-in.-diameter linear tubular solenoid and balanced counterweight and bias spring assembly is built into a module which forms the top portion of the device housing. The bottom half of the aluminum housing is an "L"-shaped piece that contains the lower half of the magnetic core and the lower pivot for the zigzag/flywheel assembly. The sensing weight guide rods and bias springs extend between the lower and upper halves of the housing. The solenoid plunger is linked to a counterweight plunger by a symmetrical, slotted steel bar, pivoted at its center. Mounted on the counterweight are the lock spring and lock pin, which interact with the flywheel to force the top half of the core either up or down, depending on whether it is in the safe or armed position. As shown in figure 9, the overall device is 1.25 $in.^2$ by 1.75 in. high with a volume of roughly 2.8 in^3. Other details of the final model are discussed in section 8.

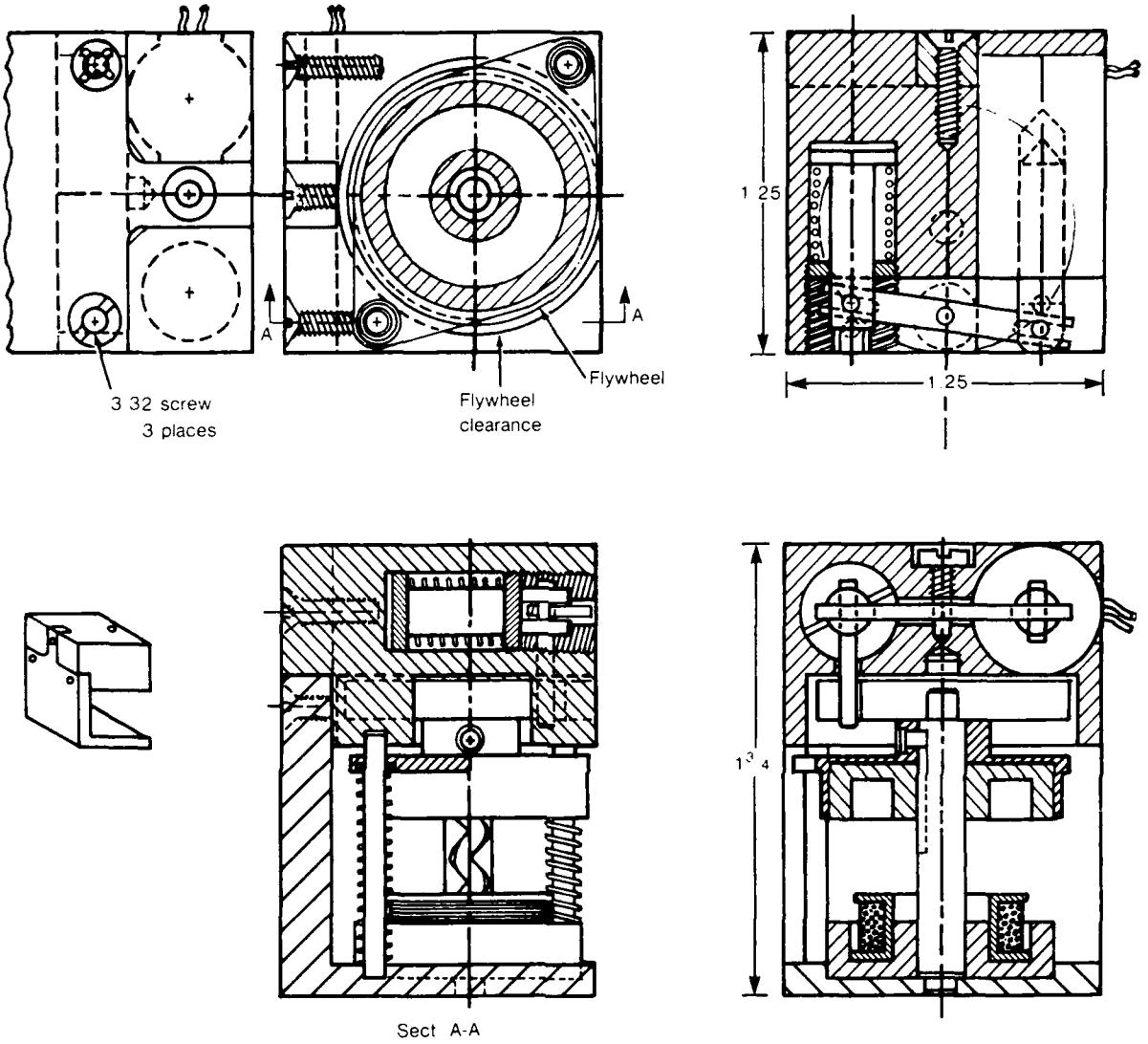

Figure 9. Selected approach.

(a) # Mechanical Data

Effective Core Set Parameters

		2311T	2318T
MAGNETIC PATH LENGTH	ℓ_e	1.19 in. 3.02 cm	1.67 in. 4.24 cm
CORE CONSTANT	$\Sigma \frac{\ell}{A}$	11.6 in.$^{-1}$ 4.57 cm^{-1}	16.7 in.$^{-1}$ 6.58 cm^{-1}
EFFECTIVE CORE AREA	A_e	.102 in.^{2} .658 cm^2	.102 in.^{2} .658 cm^2
EFFECTIVE CORE VOLUME	V_e	.122 in.^{3} 2.00 cm^3	.168 in.^{3} 2.75 cm^3
WEIGHT		.37 oz. 11.5 Grams	.53 oz. 16.5 Grams

NOTE: MINIMUM CORE AREA .484 cm^2

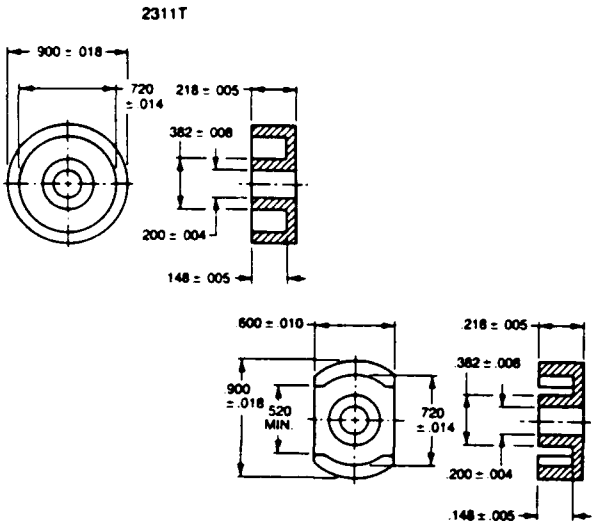

Electrical Data

Gapped Pot Cores for Frequency Selective Applications

* NON-ADJUSTABLE GAPPED POT CORE PART NO.	** ADJUSTABLE GAP POT CORE ASSEMBLY PART NO.	CORE MATERIAL	A_L† VALUE ±3%	μ_e (REF.)	APPROX. GAP LENGTH (in.)	TEMPERATURE COEFFICIENT PPM/°C	
						MIN-MAX	TEMP. RANGE
2311TA160-3B9	—	3B9 (To 300 kHz)	160	58	.023	+52 to +110	−30° to +70°C
2311TA250-3B9	—		250	91	.014	+81 to +173	
2311TA400-3B9	—		400	145	.007	+130 to +276	
2318TA160-3B9	2318TC160-3B9		160	83	.024	+74 to +158	
2318TA250-3B9	2318TC250-3B9		250	130	.015	+117 to +247	
2318TA400-3B9	2318TC400-3B9		400	209	.008	+188 to +358	

*Part number is for a core set (2 cores).
**Part number is for a core set (2 cores), nut, and specified adjustor.
†The A_L values are based on a fully wound bobbin without adjustor: mH/1000 turns.

Printed Circuit Bobbins

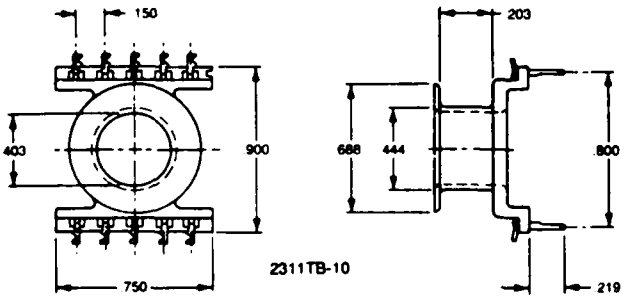

NOTE: Terminal pins are brass with hot solder precoat, dimension of pin cross section is .045" x .015".

Material: Glass filled nylon
Max. Operating Temp: 130°C
Max. Dip Soldering Temp.: 260°C for 5–6 sec.
Winding Area: .024 in.^{2} (2311) & .056 in.^{2} (2318)
Mean Length of Turn: 1.78 in.
Flammability: UL94-HB

Figure 10. Pot core data (from Ferroxcube Linear Ferrite Materials and Components Catalog, Ferroxcube Division of Amperex Electronic Corp., Saugerties, NY 12477).

(b) **3B9 Material**

This material has a linear permeability versus temperature curve from − 30 to 70°C. The low magnetic material losses and the tight tolerances on TF make this a popular ferrite for inductors and tuned transformers in the audio to 300 kHz frequency range.

By matching polystyrene capacitors with the proper 3B9 inductive device, temperature stabilities down to less than 100PPM/°C can be obtained.

Available in:
POT CORES

3B9 Characteristics

Parameters shown are typical values, based upon measurements of a medium toroidal core.

Initial Permeability at 25°C	μ_i	1800 (± 20%)
Saturation Flux Density at 25°C., H = 2 oersteds	B_s	3200 gauss*
Coercive Force	H_c	0.3 oersted*
Loss Factor at B ≤ 1 gauss	$\frac{\tan \delta}{\mu_i}$	
100 kHz		≤ 5 x 10^{-6}
500 kHz		25 x 10^{-6}*
1 MHz		120 x 10^{-6}*
Temperature Factor (− 30° to + 70°C)	TF	+ 0.9 x 10^{-6} Min. + 1.9 x 10^{-6} Max.
Disaccommodation Factor (10-100 minutes)	DF	< 2.5 x 10^{-6}
Hysteresis Loss Constant at 4 kHz	η_B	≤ 1.1 x 10^{-3} tesla^{-1}
Cune Temperature	T_c	≥ 145°C

*Typical values

Initial Permeability (μ_i) vs. Frequency

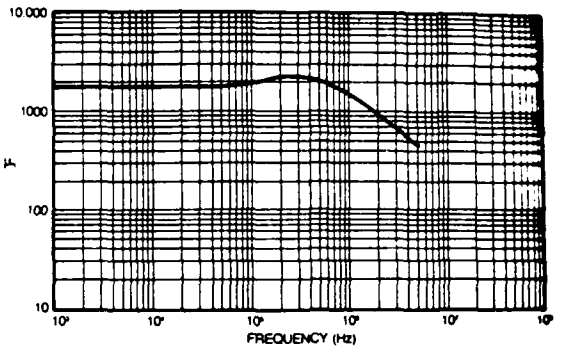

Initial Permeability (μ_i) vs. Temperature

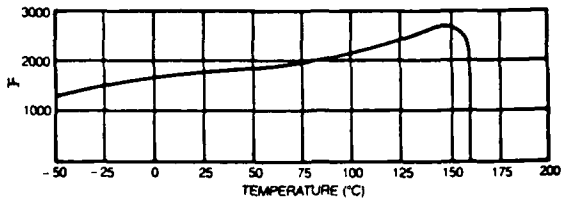

Hysteresis Curve

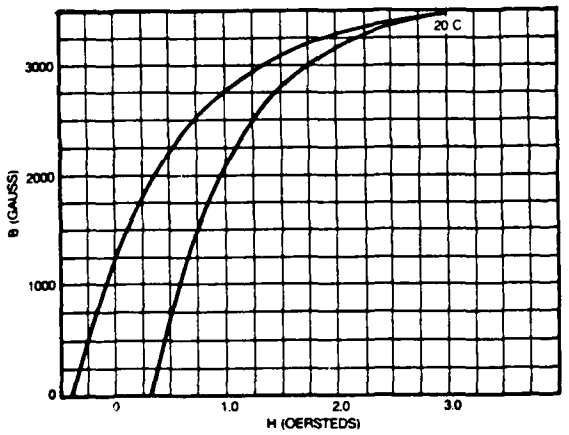

Loss Factor ($\frac{\text{Tan } \delta}{\mu_i}$) vs. Frequency

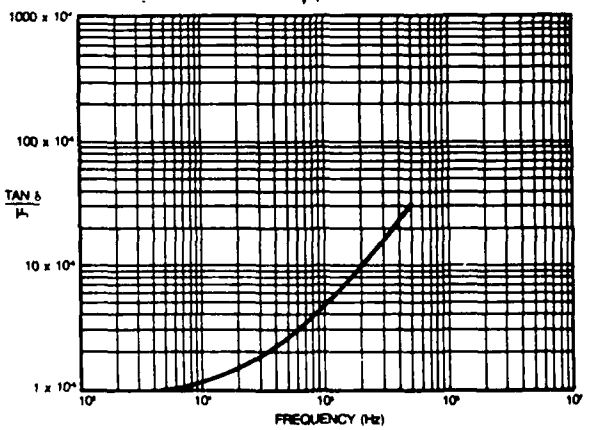

Figure 10 (cont'd). Pot core data.

6. Mechanical Analysis

The device was analyzed in two areas. Since the sensing weight and flywheel properties of the selected device can be independent, the equations used to analyze the traditional zigzag device do not apply. A new equation for this "rack and flywheel" type of device had to be generated. Second, a relation had to be established between the solenoid pull-in force and the lock spring force needed to hold the core halves together against the reset forces of the acceleration bias springs.

6.1 Equation of Motion

Appendix A gives the development of the equation of motion for this type of device. The result is

$$mC\ddot{x} + B(x + x_0) = m\left(\ddot{y} + g \sin \beta\right) \quad ,$$

where $m = W_1/g$, and

W_1 = weight of sensing weight/core assembly,

B = spring constant of acceleration spring bias system,

x = displacement of sensing weight assembly,

x_0 = initial displacement of bias springs from free position,

g = gravitational constant,

β = angle of launch with respect to local gravity

($\beta = 90°$ for vertical launch),

y = displacement of munition with respect to launcher,

$\ddot{}$ = acceleration or second derivative with respect to time,

and

C = a mechanism scaling constant,

$$C = 1 + \frac{W_2}{W_1}\left(\frac{K}{r}\right)^2\left(\frac{1 + \mu \tan \alpha}{\tan \alpha(\tan \alpha - \mu)}\right),$$

where

W_2 = weight of zigzag flywheel assembly,

K = radius of gyration of flywheel assembly,

r = radius of interaction from centerline to point where guide pin engages zigzag track,

α = helix angle of zigzag track,

and

μ = coefficient of friction between guide pin and zigzag track.

The guide pin is treated as having zero diameter, and friction is ignored at other points in the mechanism.

The only difference between this equation of motion and the one for the traditional zigzag device is the weight ratio term W_2/W_1 in the mechanism constant. This term would be unity for the traditional design and here it can be any value. The term (g sin β) is usually ignored for drop safety calculations and for high-g launch applications where it is many times smaller than the launch acceleration $\ddot{y}$. For missile applications where acceleration is approximately 20 g or less, this term should be considered when designing bias springs and when it is important to determine arming time.

The equation of motion is applied for each stage of the zigzag track, and it is assumed that the flywheel assembly comes to a complete stop before each new stage is started. Impact and bouncing between the pin and the

track are ignored. The reasonableness of these assumptions has been verified by high-speed films and airgun correlation tests done with traditional high-g zigzag mechanisms. When safety is being analyzed, it is assumed that the mass will coast through the second half of the last stage if it is driven through the first half of this stage.

6.2 Performance

An existing program to analyze the safety and performance of zigzag devices was used to evaluate performance of this design. The weight ratio of the two elements (16.3/13) was simply included with the $(k/r)^2$ ratio (0.35/0.08) when providing input to the program. Figure 11 shows the results of a safety analysis and the results of a performance analysis for a horizontal launch ($\beta = 0$) under a constant 15-g acceleration. The minimum velocity change that will arm the device is about 98 ft/s, corresponding to a free-fall drop from a height of about 150 ft. With a coefficient of friction of 0.2, the predicted arming time at 15 g is about 0.22 s.

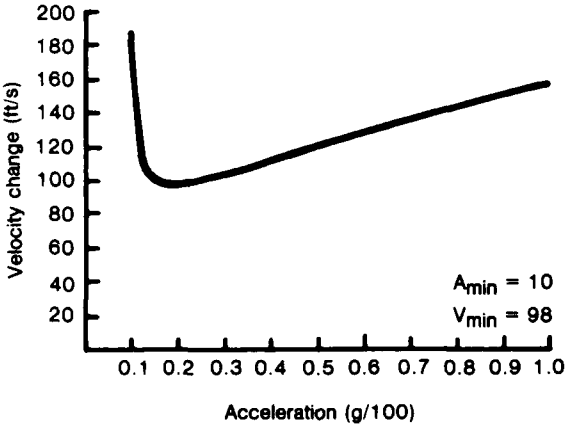

Zigzag design

1. Radius of gyration k = 0.392
2. Radius of interaction r = 0.08
3. Coeff of friction μ = 0.2
4. Number of legs N = 4

Length	angle	lead	mec-con
0.100	45	0.503	37.015
0.100	45	0.503	37.015
0.100	45	0.503	37.015
0.100	45	0.503	37.015

5. Total stroke of S/M = 0.4
6. Bias at top of stroke = 7.5
7. Bias at bottom stroke = 10.5

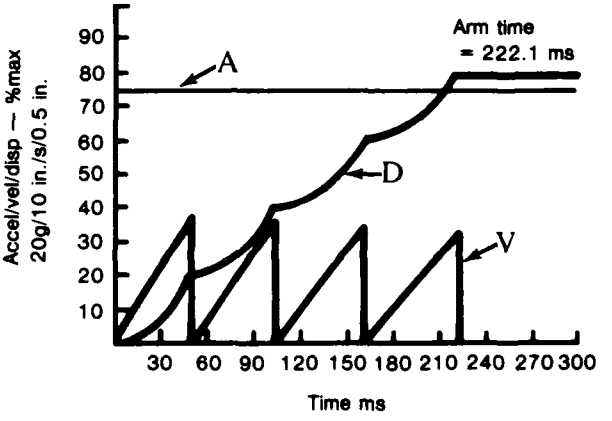

Figure 11. Analysis of zigzag transformer safety device.

6.3 Lock Spring Force Balance

In order to design the lock spring mounted on the solenoid plunger counterweight, a static force balance equation was developed. The spring must be strong enough to hold the sensing weight bias springs compressed so the transformer core halves will be clamped together in the armed position. However, the spring must not be so strong that the solenoid is incapable of pulling in against it. In addition to overcoming the force of the compressed bias springs, the lock spring must also work against the friction force between the guide pin and the zigzag track and the friction force between the lock pin and the notch in the flywheel. The analysis assumed that friction at the flywheel pivots and guide rod interfaces would be negligible. The analysis also models a design feature used to enhance the effectiveness of the lock spring: a draw-angle (delta) made in the notch in the flywheel which interlocks with the lock pin.

Results of the analysis for a horizontal orientation (assume W-0) are shown in figures 12 and 13. The second graph of figure 13 shows the effect of the draw angle on the required lock spring force when the coefficient of friction is 0.2. The first graph shows how the required spring force depends on the coefficient of friction (assumed the same at both places of interaction), for no draw-angle and for a draw-angle of 30°. Note that the moment arm ratio between the flywheel diameter and the zigzag track diameter (0.46/0.08) provides a multiplication of the lock spring force of about 4 to 1.

Based on these calculations and using a maximum acceleration bias spring force of 140 grams, a lock spring bias force of 35 grams was selected with the solenoid plunger in the starting position. A draw angle close to 0° was used on the model that was fabricated. Figure 14 shows that the Guardian tubular solenoid model #T4X7CONT24VDC (which is equivalent to the Oak Industries model C8-14) should be able to work reliably against this spring load at the established maximum gap of 0.1 in. If this solenoid could not produce the required force at 24 V, then a special drive circuit would have to be used wherein an extra high voltage would be used to pull in the solenoid plunger. Once the plunger was pulled in, the circuit would drop the voltage to the continuous 24-V level where the solenoid can hold against a load of 340 grams.

Figure 12. Analysis for lock-down force balance.

Assume:

F spring ≈ 35 gm min; 50 gm max
R_1 = 0.46
R_2 = 0.08 (R_1 R_2 = 5.75)
x = 0.375
Pivot friction = 0
Guide rod friction ≈ 0
W = 0 (horizontal acceleration)
$\beta = \cos^{-1}(X/R_1) = 35.39°$
$\alpha = 45°$
$\Psi = 90 - \beta - \delta$

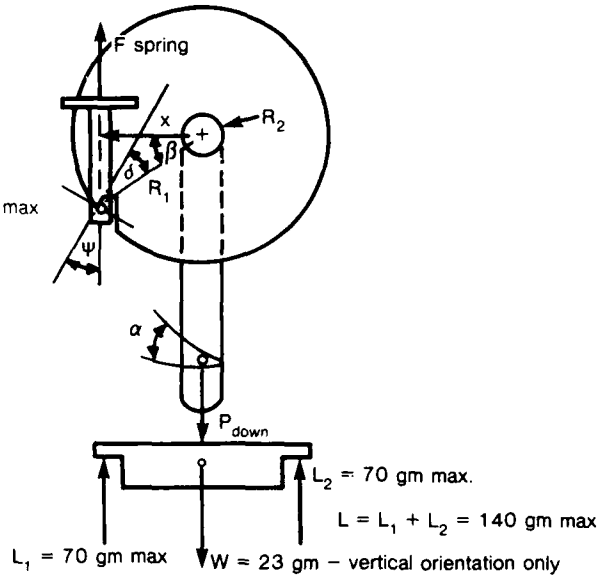

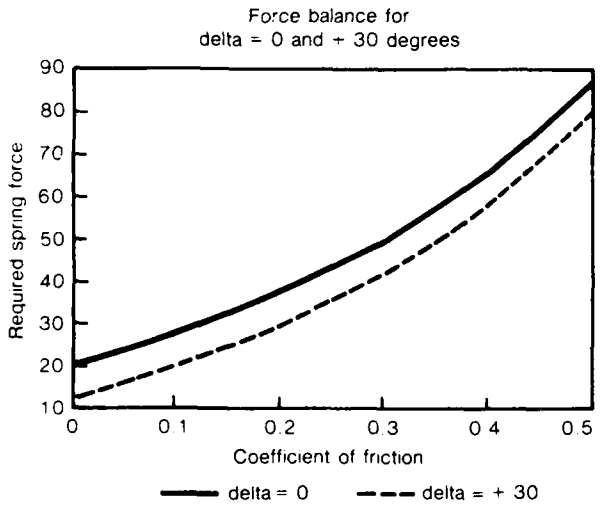

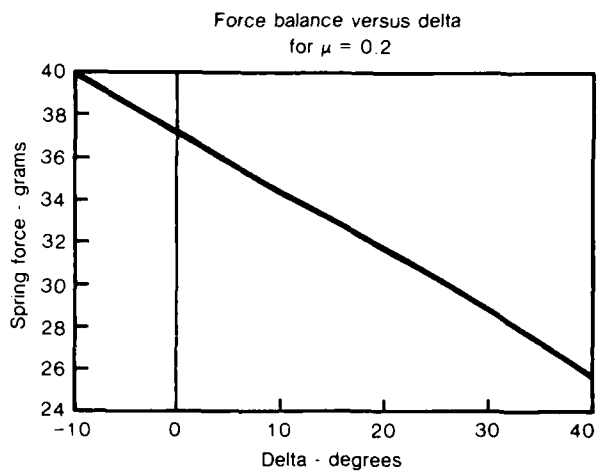

Figure 13. Results of spring force balance analysis.

ACTUAL SIZE

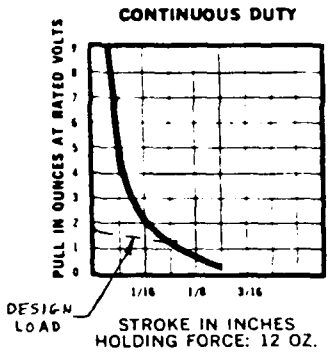

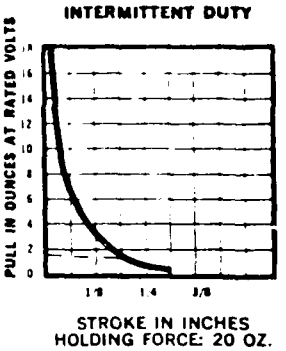

SPECIFICATIONS	
Size	½" Diameter x ⅞" Long (From Mtg. Surface)
Weight	1 Oz. Max.
Mounting	⅜-32 Threaded Bushing (Nut and Lockwasher Supplied)
Dielectric Strength	500 VRMS
Insulation Material	Class "A" (105° C)
Life Expectancy	10 Million Cycles at Rated Load
Nominal Coil Power	Continuous Duty—2.4 Watts *Intermittent Duty (10%)—7 Watts* (One Minute Max. on Time)

STANDARD COILS		
NOMINAL VOLTS (D.C.)	RESISTANCE (OHMS ± 10%) at 25°C	
	CONTINUOUS DUTY	INTERMITTENT DUTY
6	15	5
12	60	20.6
24	240	82
110	5510	1890
Other Coils and Duty Cycles Available Upon Request		

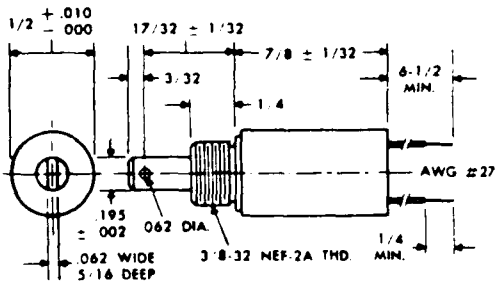

ACTUAL SIZE

Notes:
1. Solenoid shown in energized position.
2. .250 Plunger configuration shown supplied for spring return only.
3. Largest size thread that may be threaded on push rod #1.
4. Push force approximately 90% of pull forces shown.

Figure 14. Solenoid data (from Oak Industries, Inc., Crystal Lake, IL 60014).

7. Electrical Considerations

An electronic circuit to interface with the zigzag engaged pot core could reasonably use three possible transformer/inductor configurations. The most straightforward approach would be to use a push-pull forward acting transformer in a conventional dc-dc converter. Another possibility is to use the pot core as a single-ended flyback transformer. The third possibility is to use the pot core as an inductor/transformer in a resonant circuit. Two important characteristics that a selected configuration should have, even for this very limited development effort, are for operation in the open condition with very little energy transfer to the firing capacitor, and non-destructive operation. Comments by AFATL about previous work that used a separated core implemented as a conventional transformer indicated that when the circuit was operated with the core in the open position, a significant amount of energy transferred to the firing capacitor. There would be a similar problem with a flyback transformer approach. Experience with resonant circuits from a previous project and some preliminary analysis indicated that using the separated pot core as an inductor/transformer in a resonant circuit can be very effective in accomplishing the two stated design goals.

Figure 15 shows a concept for using a separated pot core as part of a fire-set voltage converter. Closed loop operation is shown with the voltage on the resonant circuit as the control parameter to anticipate the need for long charge retention on the firing capacitor in an application where the dc-dc converter turns off early in the mission. More accurate regulation can be achieved if a voltage divider can be placed across the firing capacitor and the voltage across part of this divider can be used as the control parameter. The voltage multiplier requires the use of fast switching diodes for effective operation to minimize junction charge storage. An additional diode selected for very low leakage current can be included as shown to increase charge retention time. The reason for using a tapped inductor will be discussed later. Development of a fire-set based on the concept shown in figure 15 was beyond the scope of this development effort. However, figure 16 shows a laboratory test setup which was used to evaluate the zigzag engaged pot core. Note that the test driver shown is from another project and operates at a higher frequency than desired for this application. This setup imposed limitations which will be discussed later.

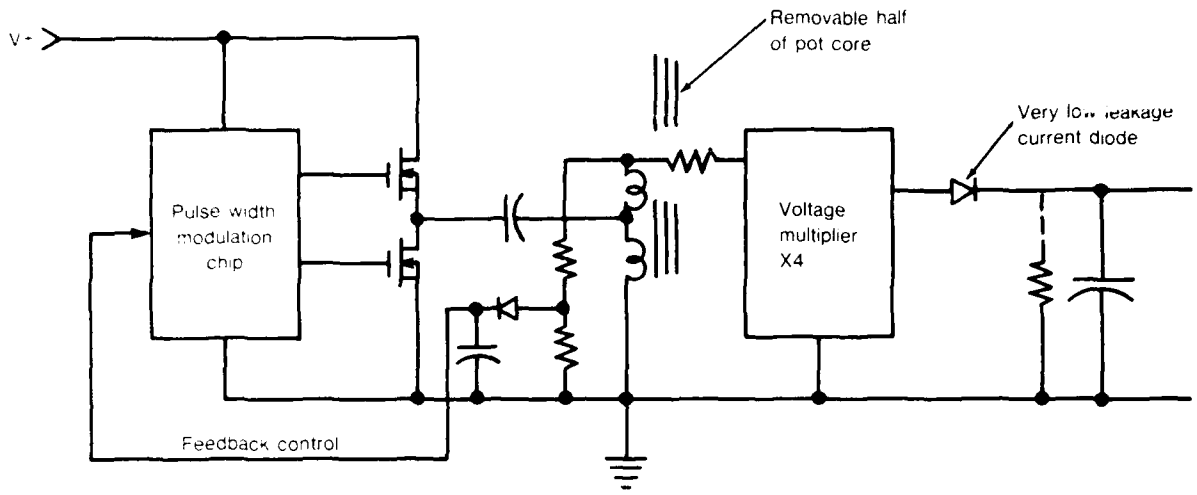

Figure 15. Fire-set with zigzag engaged pot core.

Figure 16. Laboratory test setup.

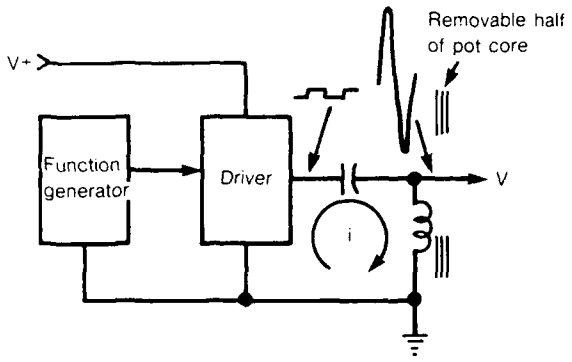

The pot core selected for this application is a Ferroxcube number 2311TA400-3B9. This core was selected because of its low profile, large center hole, correct size, and availability as a sample. The characteristics of this core, other than dimensions, are

A_L = 400 mH/1 K turns = inductance index,
μ = 145 = permeability,
Gap = 0.007 in. = core center gap,
A_e = 0.658 cm^2 = equivalent x-sect. area of core,
l_e = 3.02 cm = equivalent magnetic path length,
V_e = 2.00 cm^3 = volume of core, and
Weight = 11.5 grams = weight of core.

If we use an operating frequency of 100 kHz and a power dissipation of 1 W, the peak flux density (B_{max}) is about 1300 gauss. To calculate the minimum number of turns (N) needed to control flux density at this level, Faraday's law can be used with E_{rms} = 500 V.

$$B_{max} = E_{rms} \times 10^8/4.44\ A_e NF.$$

or

$$N = E_{rms} \times 10^8/4.44\ A_e F B_{max} = 500 \times 10^8/4.44 \times 0.658 \times 10^5 \times 1.3 \times 10^3$$
$$= 131 \text{ turns, where F = frequency.}$$

To provide flexibility for operation at frequencies well below 100 kHz, N can be increased to 150 turns. A scramble-wound winding of 150 turns of #32 wire will comfortably fill the bobbin. The inductance of the winding can be calculated from the value of A_L.

$$\text{Inductance L (mH)} = A_L N^2 \times 10^{-6} = 400 \times 150^2 \times 10^{-6} = 9 \text{ mH.}$$
$$\text{Reactance } X_L \text{ (100 kHz)} = 2\pi FL = 6.28 \times 10^5 \times 9 \times 10^{-3} = 5.7 \text{ k}\Omega.$$

With the core in the zigzag assembly, the measured values are 6.33 mH closed, 0.68 mH open, and a resistance of 3.8 Ω. In the closed position, the core halves do not quite mate together. Shown in figure 17 is a plot of inductance versus measured separation distance. Clearly, the inductance changes very rapidly with separation distance when the core halves are near each other. The inductance was measured for 15 hand closures with the inductance typically varying from 6 to 8 mH, with some values outside this range. Centrifuge test results might be more consistent. The wide range of inductances in the closed position is probably too great for use with any of the three possible transformer/inductor configurations mentioned earlier. However, a core with a larger air gap and mechanical design changes may reduce this inductance range to an acceptable level.

The effect that resonance can have on circuit operation in the closed and open positions can be illustrated by comparing the reactances for these conditions. For component values of L = 6.5 to 7.0 mH, C = 500 pF, and a resonant frequency in the range from 85 to 90 kHz, these reactances are shown in figure 18. In the closed position, the reactances nearly cancel

Figure 17. Inductance versus separation distance.

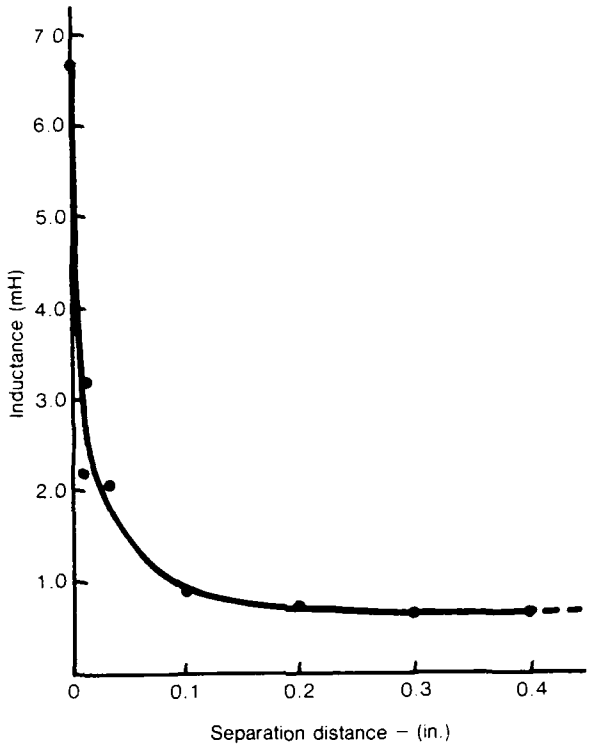

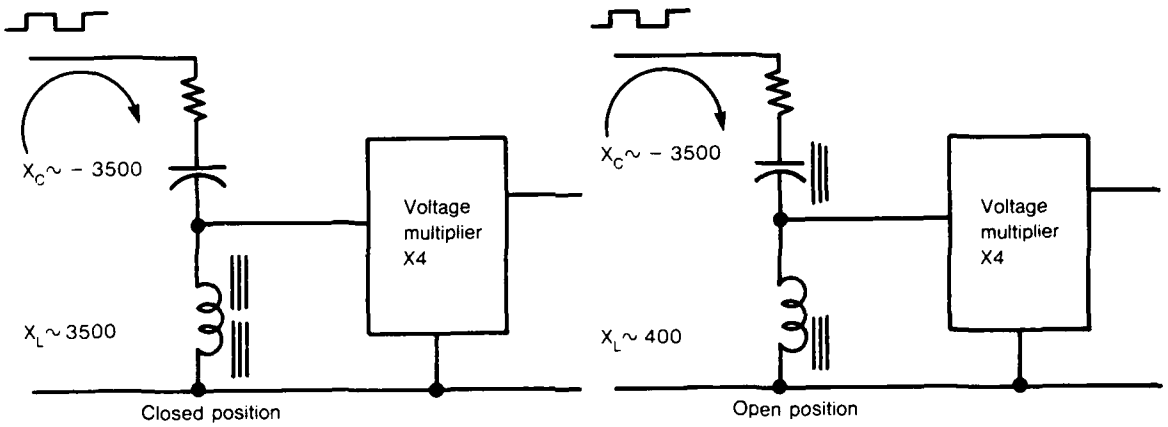

Figure 18. Comparison of impedances.

and the circuit has a relatively low impedance with relatively high circulating current. In the open position, this situation changes dramatically and can be summarized as follows:

(a) Resonant action stops.
(b) The impedance of the circuit greatly increases.
(c) The circulating current decreases to a very low value.
(d) The voltage divider formed between X_C and X_L greatly attenuates the voltage across L and to the voltage multiplier.

Shown in figure 19 are traces of the voltage across and current through L for the closed and open positions when using the laboratory test setup of figure 16. In the closed position, the voltage into the voltage multiplier is approximately 500 Vrms, and in the open position this voltage is approximately 10 Vrms. In a fire-set application, losses in the voltage multiplier and a bleed resistor would attenuate this voltage to an even lower value. The third set of traces in figure 19 shows the effect of retuning the frequency source to establish resonance in the open position. In this case the frequency is approximately 280 kHz and the voltage into the voltage multiplier would be approximately 25 Vrms. This low voltage at resonance in the open position indicates a greatly reduced Q under these conditions. This change in Q is expected since the coil is acting partly as an air core inductor. The value of Q in the closed position is about 20 and in the open position is approximately 2. The driver used in the setup of figure 16 was designed to operate at 500 kHz. If this driver were redesigned to operate at 85 to 90 kHz with a clean drive waveform, the traces in figure 19 would be low distortion sine waves.

The large variation in inductance in the closed position creates a serious problem for using a zigzag engaged pot core in an electronic circuit, particularly as part of a resonant circuit. Improvements in the mechanical design, increasing the length of the air gap, and possibly selecting a core with a better magnetic profile are modifications which could reduce this variation. It is not recommended that dual control parameters (servo action to adjust both frequency and duty factor) be used to tune the frequency source to the resonant frequency of the LC circuit. However, using only frequency as the control parameter is a viable possibility as long as safety issues are properly considered. Passive matching of the frequency source to the resonant frequency of the LC circuit, if this approach

is used, will require a variation of inductance in the closed position of 5 to 10 percent. In addition, a low Q of 5 to 10 will also be required.

Figure 19. Waveforms.

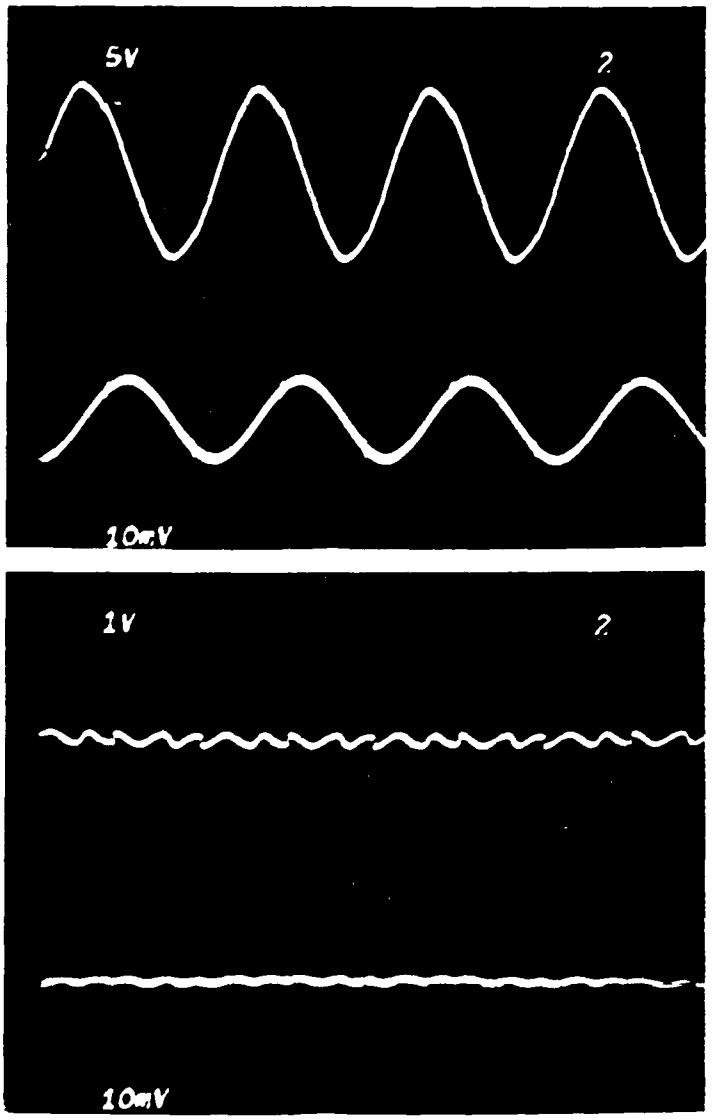

Figure 19 (cont'd). Waveforms.

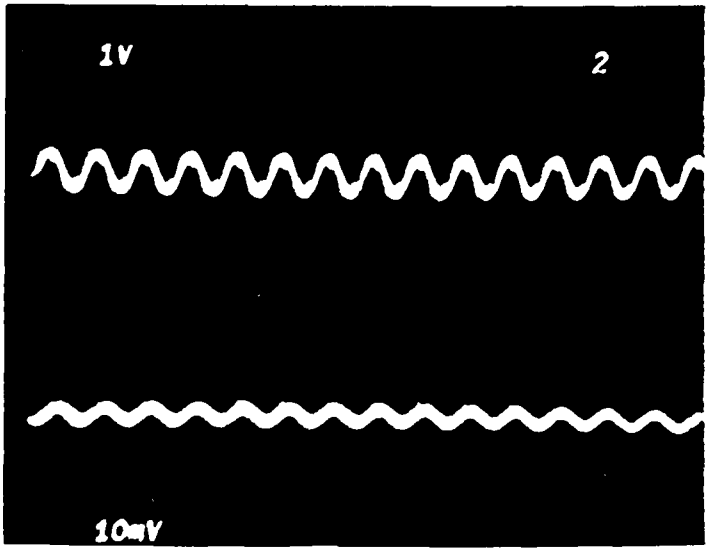

The tapped inductor shown in figure 15 will provide transformer action to generate an adequately high voltage with a low-Q LC circuit. The turns ratio of this tapped inductor would typically be about 2 to 10, and the reflected winding capacitance would have little effect on circuit operation. The resistor between the LC circuit and the voltage multiplier will isolate the LC circuit from parasitic diode junction capacitances. The real power losses in a low-Q LC circuit do not necessarily have to be substantial. Intermittent circuit operation is a technique for reducing losses. In a fully developed fire-set using a zigzag engaged pot core, the required charging time of the firing capacitor, operating frequency, LC circuit impedances, and circulating current can all be traded off to optimize the design.

8. Model and Tests

Figures 20 to 22 show the model which was built. Its design is reflected in the drawings of appendix B. Most of the design has been described earlier. Note the use of miniature ball-bearings on each end of the zigzag shaft and flywheel assembly. The final assembly is also about 0.09-in. taller than the desired 1.75 in. This extra height was used to prevent breakout of the half-inch-diameter hole for the solenoid as shown in figure 9, and to cover the lower ball-bearing which was installed after the other parts had been fabricated. The unusual "T"-shaped interface between the top and bottom sections of the housing was used in place of dowel pins since the assembly screws used the space needed for dowel pins. The guide pins for the bias springs on the sensing weight were changed to threaded screws that could be inserted through the housing's bottom to

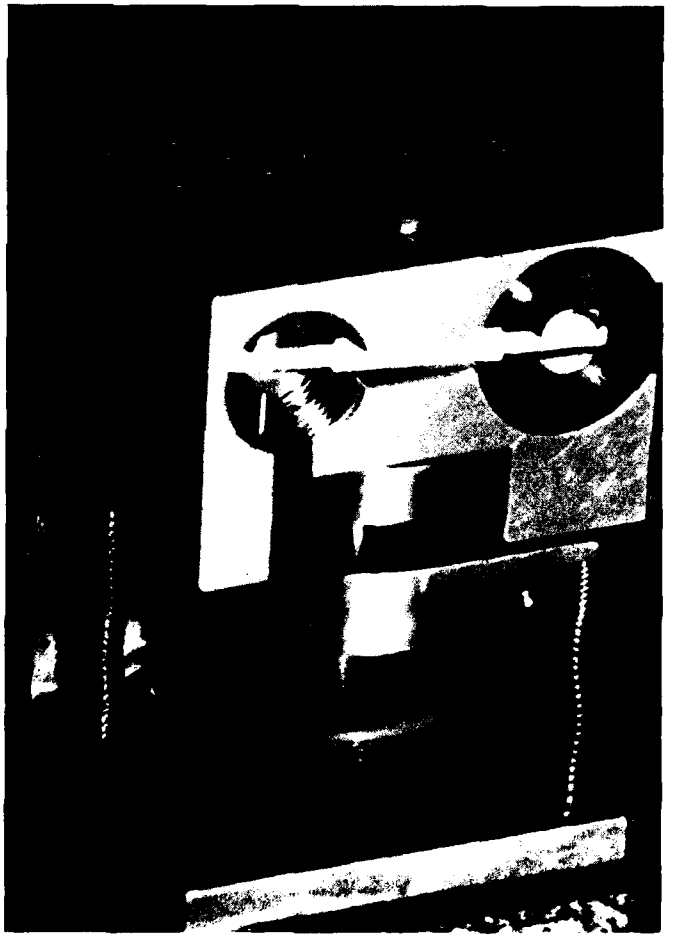

Figure 20. Zigzag model from left front.

ease final assembly. The link-bar between the solenoid plunger and its counterweight was made to have a closer fit in the housing than shown in figure 9 in order to make the interface between the lock pin and the flywheel more rigid. The clutch feature shown in figures 6 and 8 was not incorporated in the model. A single coil of wire is used on the magnetic core's bobbin because the preliminary intent was to use the system as a resonant inductor type of converter circuit. Two independent coils or a tapped coil transformer type of system can be explored by simply replacing the present coil assembly.

Figure 21. Zigzag model from upper right, armed.

Figure 22. Zigzag model from lower right.

The purpose of this project was to illustrate the feasibility of a new concept for a safety device. The model as a visualization piece does this, so extensive testing of the model was not required. Some electrical tests were done, as described in the previous section, and some centrifuge tests were done to demonstrate proper operation in an acceleration field. Results of the tests using a centrifuge radius of 10.5 in. are summarized in table 1 and in figure 23.

On the basis of four runs, the tests show that the weight starts to move down at a level of 8 to 9 g, and it bottoms out at 9 to 10 g. On reset, the weight begins to move back up at 5.5 to 7 g and is fully reset at 3.5 to 4.5 g. The difference between the arming and reset levels is due to friction in the mechanism. Three dynamic tests from preset g-levels showed that the unit did not arm at less than 9 g and did arm above 9 g.

Table 1. Centrifuge Test Results

Centrifuge radius--safe position: 10.25 in.
Centrifuge radius--armed position: 10.75 in.

Test A: Preactivate solenoid; slowly increase centrifuge speed; observe motion of weight.

Run	Wt. starts motion (g)	Wt. at bottom (g)	Wt. starts reset (g)	Wt. fully reset (g)
1	8.4	9.0	5.7	3.5
2	8.9	9.8	6.6	4.2
3	8.4	9.4	6.6	4.2
4	8.9	10.1	6.1	4.2
Avg	8.65	9.58	6.25	4.02

Test B: Preset centrifuge speed; activate solenoid; observe arming.

Run	g-level	Result
1	8.4	No-arm
2	8.9	No-arm
3	9.4	Armed

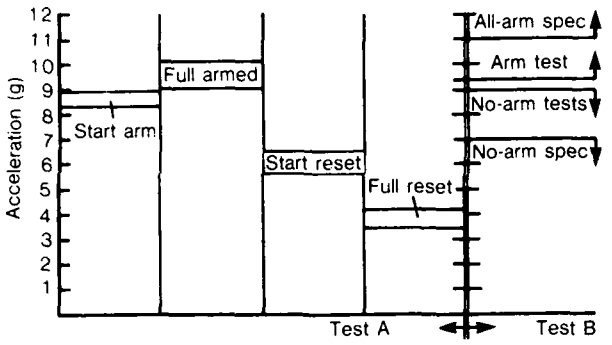

Figure 23. Centrifuge test results.

Two other things were noted during the testing. First, the clearance between the sensing weight and the zigzag shaft was too great, so the weight tended to cock and jam in the safe position where the cam track does not run out at the top of the shaft. Adding shims to the top of the weight, so that it starts out properly aligned, eliminated the jamming problem. Second, the solenoid performed sluggishly when trying to pull in against friction created by the acceleration load. This was not taken into account in either the design or the analysis. Both the plunger and the counter weight, and the link-bar, have to slide (or rotate) while being pressed down by the g-force. Well polished and lubricated surfaces could help this situation, but the loading cannot be eliminated where a linear solenoid is used in a module oriented on top of the flywheel as in this design. Note that the configuration shown in figure 7, where the solenoid and counterweight system is mounted vertically behind the unit so as to move in the same plane as the g-field, can be made essentially immune to friction loading by acceleration. In the actual missile application, the solenoid would probably be actuated before the drive acceleration is applied. Thus, the friction problem occurs only in laboratory testing.

9. Conclusions

Within the constraints of limited funding and time budgets, this project has demostrated the practicality of constructing a zigzag device to provide safety and arming for a high voltage converter system. Mechanically, the first model works very well and shows that there should be no barriers to the development of reliable production hardware. There are still some reservations about electrical performance as discussed in section 7. The present design has only about 20 parts. Various mechanical design refinements should be considered as discussed in the recommendations, section 10. Care must be taken to ensure that the core halves are clamped tightly together in the armed position, and that the interaction between the sensing weight and the zigzag shaft is very smooth. The magnetic core used in this design is a large one and it should have the capacity to supply fairly large firing systems. Smaller cores and flywheels should be easy to implement, but shrinking the size of the solenoid locking system will probably be difficult.

10. Recommendations

These recommendations apply primarily to the mechanical design for construction of a second prototype model of the same basic configuration as the first model.

(a) Make the zigzag post of stainless steel instead of aluminum. Have the cam track extend high enough so that the sensing weight stops against the solenoid module housing (see item (h) below) instead of having the guide pin stop against the end of the track. Also, optimize the clearance between the post and the hole in the moving weight.

(b) Make the zigzag post long enough to include the pivot on each end and to have a "D"-shaped shoulder for attaching a flywheel having a "D"-shaped hole in its center. Also, make the diameter of the shaft slightly bigger so as to fit closer to the hole in the transformer cores.

(c) Design the flywheel with a "rim-and-disk" configuration which optimizes its inertia-to-weight ratio. This optimum design occurs when the inside radius of the rim is made about 80 percent of its outside radius.

(d) Devise a scheme for adjusting the position of the lock-pin notch in the flywheel edge relative to the position of the zigzag track. This might take the form of a rotatable rim on the flywheel which can be clamped in a position which gives the best locking action in both the safe and armed positions.

(e) Configure the mounting of the transformer core and ball-bearing in the lower housing so that the bearing does not protrude through the bottom of the unit.

(f) Extend the last stage of the zigzag track so that the guide pin in the sensing weight is still on a sloping surface of the track when the core halves come together. The guide pin rests in a crotch of the zigzag track at the armed position of the first model, so no excess clamping force is available to hold the core halves tightly together.

(g) To enhance performance during centrifuge testing, reduce the effect of acceleration-induced friction in the solenoid and counterweight module by using a Teflon-impregnated plunger liner, polishing surfaces, using dry film lubricants, minimizing contact area on the link-bar, etc.

(h) Design the sensing weight with projections above the guide pin holes so that these projections stop the weight's upward motion by resting against the underside of the solenoid housing. This will help lock the weight much more rigidly in the safe position and protect against damage during vibration testing.

(i) Consider adding a third piece to the housing assembly in order to make the zigzag mechanism a module independent of the solenoid/counter weight module. This would be done only if the current configuration is deemed too difficult to assemble.

(j) Consider reconfiguring the solenoid locking module to mount on the back or side face of the unit so the height is reduced and the module is less subject to friction during acceleration, as mentioned at the end of section 8. This will possibly complicate its interface with the flywheel.

APPENDIX A.--Development of Equations of Motion for Helix-Driven Flywheel Device

A Lagrangian method is used to develop the equations of motion based on the illustration of figure A-1. This device is similar to a flywheel and pinion driven by a translating gear rack, except the rack and pinion are replaced by a fast-lead screw thread. Friction is accounted for only at the point of interaction between the driving and driven members. Friction between each member and its guide or bearing surfaces is ignored.

Figure A-1. Schematic of helix-driven flywheel device.

Note: illustration is schematic;
α actually remains constant during motion.

coordinates X_2 and X_3 are used to account for friction.

β = angle of launch.

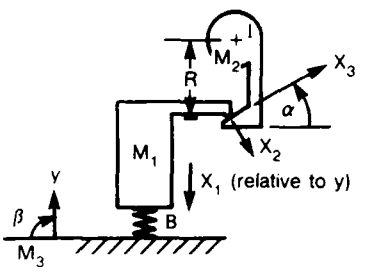

$$\text{Kinetic energy } T = \frac{1}{2} m_3 \dot{y}^2 + \frac{1}{2} m_1 \left(\dot{y} - \dot{x}_2 \cos \alpha + x_3 \sin \alpha \right)^2 \tag{A-1}$$

$$+ \frac{1}{2} I \left(\frac{\dot{x}_3 \cos \alpha}{R} + \frac{\dot{x}_2 \sin \alpha}{R} \right)^2 .$$

$$\text{Potential energy } V = m_3 g y \sin \beta + m_1 g \sin \beta (y - x_2 \cos \alpha + x_3 \sin \alpha) \tag{A-2}$$

$$+ \frac{1}{2} B (x_2 \cos \alpha - x_3 \sin \alpha + x_0)^2 .$$

APPENDIX A

$$\text{Lagrangian } L = T - V = \frac{1}{2} m_3 \dot{y}^2 + \frac{1}{2} m_1 \dot{y}^2 + \frac{1}{2} m_1 \dot{x}_2^2 \cos^2 \alpha + \frac{1}{2} m_1 \dot{x}_3^2 \sin^2 \alpha$$

$$- m_1 \dot{y}\, \dot{x}_2 \cos \alpha + m_1 \dot{y} \dot{x}_3 \sin \alpha - m_1 \dot{x}_2 \cos \alpha\, \dot{x}_3 \sin \alpha \qquad \text{(A-3)}$$

$$+ \frac{1}{2} \frac{I}{R^2} \dot{x}_3^2 \cos^2 \alpha + \frac{1}{2} \frac{I}{R^2} \dot{x}_2^2 \sin^2 \alpha + \frac{I}{R^2} \dot{x}_3 \cos \alpha\, \dot{x}_2 \sin \alpha$$

$$- m_3 g y \sin \beta - m_1 g \sin \beta\, (y - x_2 \cos \alpha + x_3 \sin \alpha)$$

$$- \frac{1}{2} B x_2^2 \cos^2 \alpha - \frac{1}{2} B x_3^2 \sin^2 \alpha - \frac{1}{2} B x_0^2 + B x_2 \cos \alpha\, x_3 \sin \alpha$$

$$- B x_2 \cos \alpha\, x_0 + B x_3 \sin \alpha\, x_0 \ .$$

$$\frac{d}{dt}\left(\frac{\delta L}{\delta \dot{y}}\right) = m_3 \ddot{y} + m_1 \ddot{y} - m_1 \ddot{x}_2 \cos \alpha + m_1 \ddot{x}_3 \sin \alpha \ . \qquad \text{(A-4)}$$

$$\frac{d}{dt}\left(\frac{\delta L}{\delta \dot{x}_2}\right) = m_1 \ddot{x}_2 \cos^2 \alpha - m_1 \ddot{y} \cos \alpha - m_1 \ddot{x}_3 \cos \alpha \sin \alpha + \frac{I}{R^2} \ddot{x}_2 \sin^2 \alpha \qquad \text{(A-5)}$$

$$+ \frac{I}{R^2} \ddot{x}_3 \cos \alpha \sin \alpha \ .$$

$$\frac{d}{dt}\left(\frac{\delta L}{\delta \dot{x}_3}\right) = m_1 \ddot{x}_3 \sin^2 \alpha + m_1 \ddot{y} \sin \alpha - m_1 \ddot{x}_2 \cos \alpha \sin \alpha + \frac{I}{R^2} \ddot{x}_3 \cos^2 \alpha \qquad \text{(A-6)}$$

$$+ \frac{I}{R^2} \ddot{x}_2 \cos \alpha \sin \alpha \ .$$

$$\frac{\delta L}{\delta Y} = -m_3 g \sin \beta - m_1 g \sin \beta \ . \qquad \text{(A-7)}$$

$$\frac{\delta L}{\delta x_2} = + m_1 g \cos \alpha \sin \beta - B x_2 \cos^2 \alpha + B x_3 \cos \alpha \sin \alpha - B x_0 \cos \alpha \ . \qquad \text{(A-8)}$$

$$\frac{\delta L}{\delta x_3} = -m_1 g \sin \alpha \sin \beta - B x_3 \sin^2 \alpha + B x_2 \cos \alpha \sin \alpha + B x_0 \sin \alpha \ . \qquad \text{(A-9)}$$

The constraint equation is $\ddot{x}_2 = \dot{x}_2 = x_2 = 0$. (A-10)

The constraint force in the x_2 direction $= \lambda$. (A-11)

The constraint force in the x_3 direction $= -\mu\lambda$. (A-12)

The resulting equations of motion are

$$\frac{d}{dt}\left(\frac{\delta L}{\delta \dot{y}}\right) - \frac{\delta L}{\delta y} = F(t) = (m_1 + m_3)\ddot{y} + m_1 \ddot{x}_3 \sin\alpha + (m_1 + m_3)\, g \sin\beta \ . \tag{A-13}$$

$$\frac{d}{dt}\left(\frac{\delta L}{\delta \dot{x}_2}\right) - \frac{\delta L}{\delta x_2} = \lambda = m_1\left(-\ddot{x}_3 \sin\alpha\cos\alpha - \ddot{y}\cos\alpha\right) + \frac{I}{R^2}\ddot{x}_3 \sin\alpha\cos\alpha$$
$$- m_1 g \cos\alpha \sin\beta + B\left(-x_3 \sin\alpha\cos\alpha + x_0 \cos\alpha\right) \ , \tag{A-14}$$

and

$$\frac{d}{dt}\left(\frac{\delta L}{\delta \dot{x}_3}\right) - \frac{\delta L}{\delta x_3} = -\mu\lambda = m_1\left(\ddot{x}_3 \sin^2\alpha + \ddot{y}\sin\alpha\right) + \frac{I}{R^2}\ddot{x}_3 \cos^2\alpha$$
$$+ m_1 g \sin\alpha \sin\beta + B\left(x_3 \sin^2\alpha - x_0 \sin\alpha\right) \ . \tag{A-15}$$

Combine equations (A-14) and (A-15) to eliminate λ and obtain

$$m_1\left(\ddot{x}_3 \sin^2\alpha + \ddot{y}\sin\alpha\right) + \frac{I}{R^2}\ddot{x}_3 \cos^2\alpha + m_1 g \sin\alpha \sin\beta$$
$$+ B\left(x_3 \sin^2\alpha - x_0 \sin\alpha\right) = -\mu\left[m_1\left(-\ddot{x}_3 \sin\alpha\cos\alpha - \ddot{y}\cos\alpha\right)\right. \tag{A-16}$$
$$\left. + \frac{I}{R^2}\ddot{x}_3 \sin\alpha\cos\alpha - m_1 g \cos\alpha \sin\beta + B\left(-x_3 \sin\alpha\cos\alpha + x_0\cos\alpha\right)\right] .$$

APPENDIX A

Rearranging

$$\ddot{x}_3\left[m_1\left(\sin^2\alpha-\mu\sin\alpha\cos\alpha\right)+\frac{I}{R^2}\left(\cos^2\alpha+\mu\sin\alpha\cos\alpha\right)\right]$$
$$+B\left[x_3\left(\sin^2\alpha-\mu\sin\alpha\cos\alpha\right)-x_0\left(\sin\alpha-\mu\cos\alpha\right)\right] \tag{A-17}$$
$$=-m_1 g\sin\beta\left(\sin\alpha-\mu\cos\alpha\right)-m_1\ddot{y}\left(\sin\alpha-\mu\cos\alpha\right)\ .$$

Divide by $\sin\alpha-\mu\cos\alpha$:

$$\ddot{x}_3\left[m_1\sin\alpha+\frac{I}{R^2}\left(\frac{\cos^2+\mu\sin\alpha\cos\alpha}{\sin\alpha-\mu\cos\alpha}\right)\right]+B\left(x_3\sin\alpha-x_0\right) \tag{A-18}$$
$$=-m_1\left(\ddot{y}+g\sin\beta\right)\ .$$

Note that $x_1=-x_3\sin\alpha$ and substitute in (A-18) to obtain

$$-m_1\ddot{x}_1-\ddot{x}_1\frac{I\cos\alpha}{R^2\sin\alpha}\left(\frac{\cos\alpha+\mu\sin\alpha}{\sin\alpha-\mu\cos\alpha}\right)-B\left(x_1+x_0\right)=-m_1\left(\ddot{y}+g\sin\beta\right)\ . \tag{A-19}$$

Multiply by -1; rearrange using $\tan\alpha=\frac{\sin\alpha}{\cos\alpha}$, and drop the subscript on x_1 to obtain

$$m_1\ddot{x}\left(1+\frac{I}{m_1R^2}\left(\frac{1+\mu\tan\alpha}{\tan\alpha\left(\tan\alpha-\mu\right)}\right)\right)+B\left(x+x_0\right)=m_1\left(\ddot{y}+g\sin\beta\right)\ . \tag{A-20}$$

Note that $I=m_2K^2$.

$$\text{Let } C = 1 + \frac{W_2}{W_1}\left(\frac{K}{R}\right)^2\left(\frac{1+\mu\tan\alpha}{\tan\alpha\,(\tan\alpha-\mu)}\right) . \tag{A-21}$$

$$\text{Then } mC\ddot{x} + B(x+x_0) = m\left(\ddot{y} + g\sin\beta\right) , \tag{A-22}$$

where $m = \frac{W_1}{g}$.

APPENDIX B.--Design Drawings

The drawings of the acceleration sensing mechanism discussed in the body of this report are shown in this appendix (fig. B-1 to B-16) and reflect the model which was built at Harry Diamond Laboratories (HDL). The final design is shown in figures 20 to 22, body of report. The model is fully described in the text, especially in sections 5 and 8, body of report.

The assembly drawing (fig. B-1) does not accurately reflect all final details. Drawings 11730837 and 11730838 (fig. B-12 and 13) are not detailed to show the ball-bearing seats in the frame and housing.

List of Drawings

Number	Part	Figure No.
None	Assembly details	B-1
11733741-Sh 1	Post, zigzag	B-2(a)
11733741-Sh2	Post, zigzag	B-2(b)
11733743	Pin, setback	B-3
11730829	Modifications for zigzag post	B-4
11730830	Bias spring	B-5
11730831	Lock spring	B-6
11730832	Actuator link	B-7
11730833	Guide rod	B-8
11730834	Solenoid modifications	B-9
11730835	Core holder	B-10
11730836	Flywheel	B-11
11730837	Frame	B-12
11730838	Housing	B-13
11730840	Piston	B-14
11730841	Retainer	B-15
11730842	Pin, piston, and solenoid	B-16

APPENDIX B

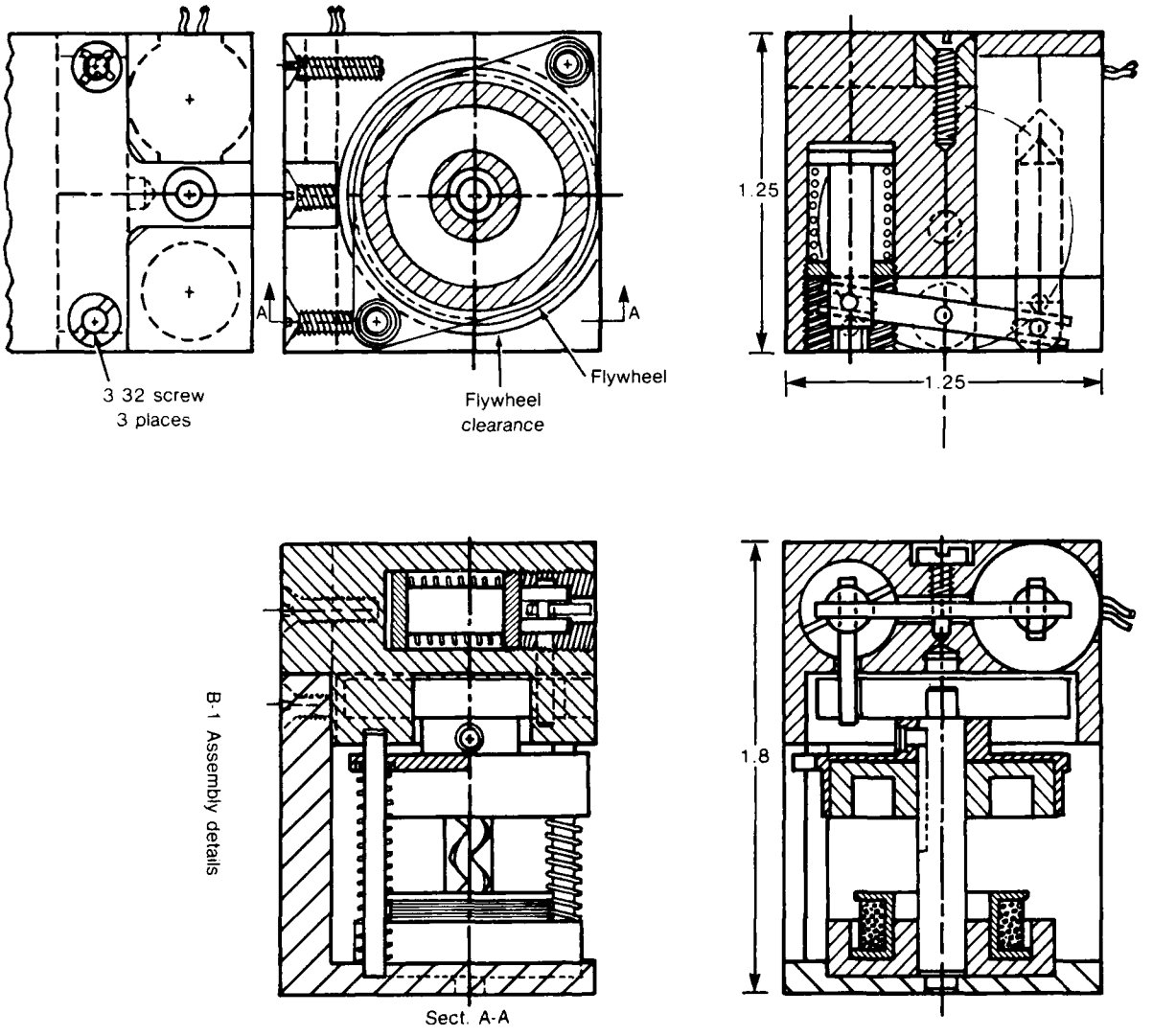

Figure B-1. Assembly details.

Figure B-2. Post, zigzag.

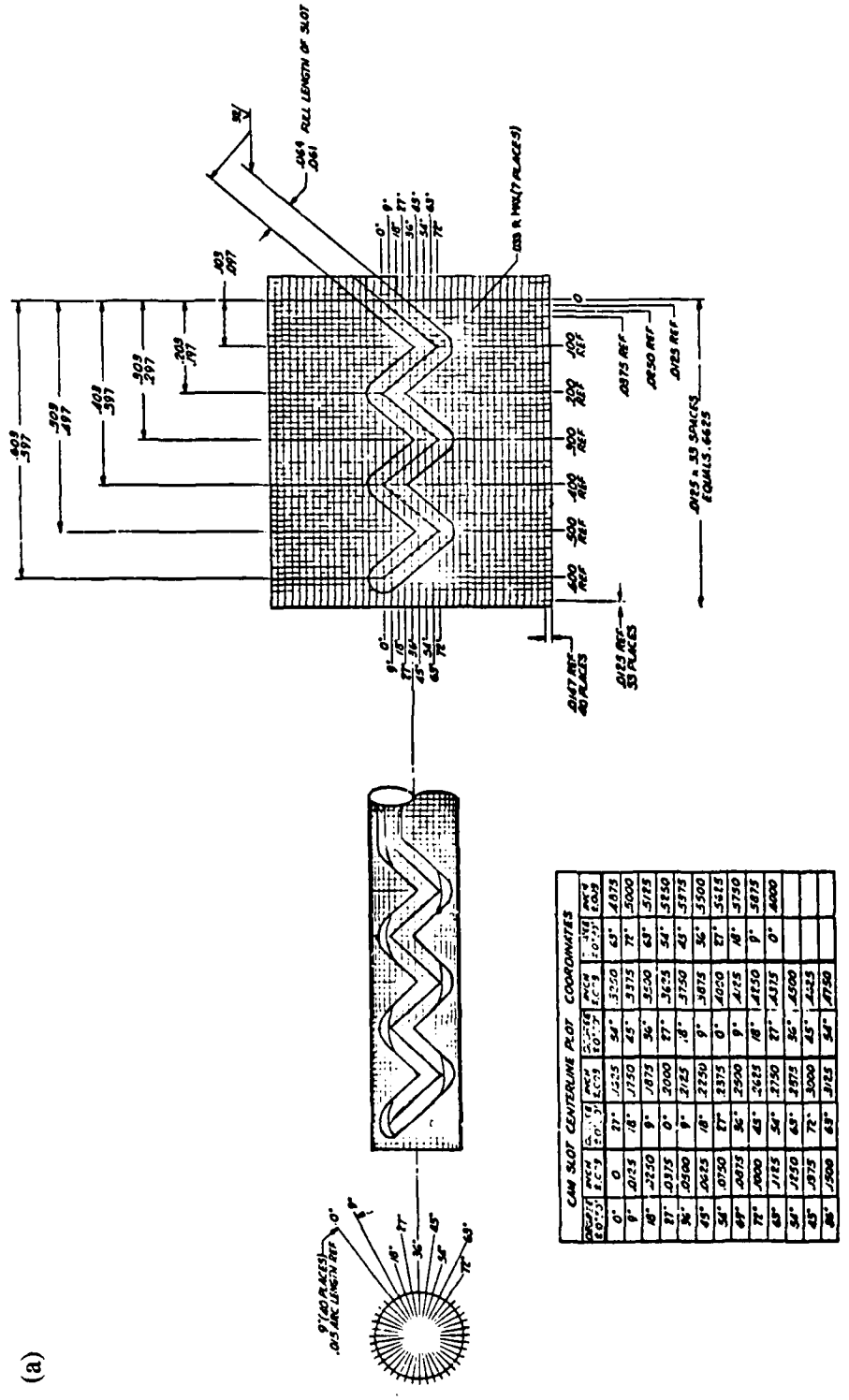

DEGREES	INCH	DEGREES	INCH	DEGREES	INCH
0°	0	11°	.1225	54°	.3250
9°	.0125	18°	.1150	45°	.3375
18°	.0250	9°	.1875	36°	.3500
11°	.0375	0°	2000	27°	.3625
36°	.0500	9°	.2125	18°	.3750
45°	.0625	18°	.2250	9°	.3875
54°	.0750	11°	.2375	0°	.4000
69°	.0875	36°	.2500	9°	.425
72°	.1000	45°	.2625	18°	.4250
63°	.1125	54°	.2750	11°	.4375
54°	.1250	63°	.2875	36°	.4500
45°	.1375	72°	.3000	45°	.4625
36°	.1500	63°	.3125	54°	.4750
27°	.1625	54°	.3250	63°	.4875
18°	.1750	45°	.3375	72°	.5000
9°	.1875	36°	.3500	63°	.5125
0°	.2000	27°	.3625	54°	.5250
9°	.2125	18°	.3750	45°	.5375
18°	.2250	9°	.3875	36°	.5500
11°	.2375	0°	.4000	27°	.5625
36°	.2500	9°	.425	18°	.5750
45°	.2625	18°	.4250	9°	.5875
54°	.2750	11°	.4375	0°	.6000
63°	.2875	36°	.4500		
72°	.3000	45°	.4625		
63°	.3125	54°	.4750		

(a)

APPENDIX B

Figure B-2 (cont'd).
Post, zigzag.

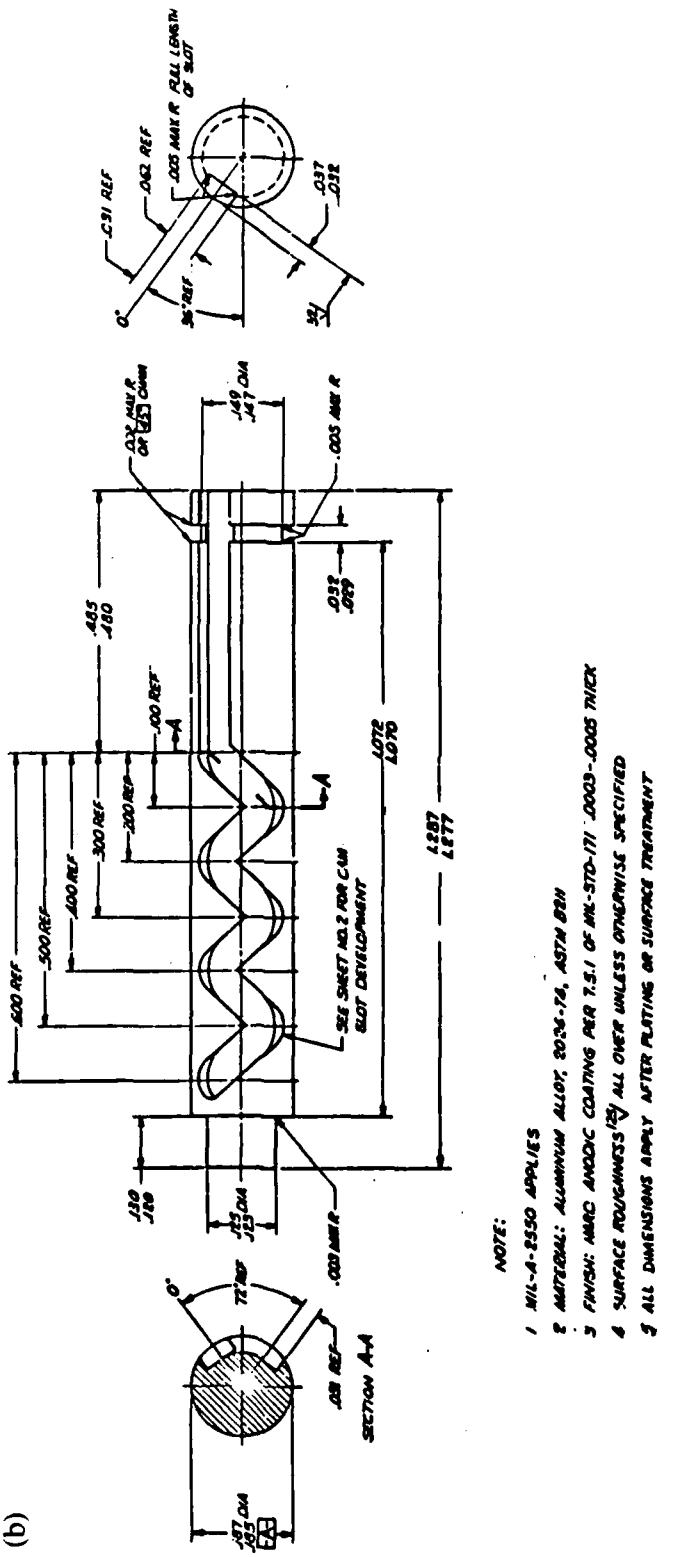

Figure B-3. Pin, setback.

1 MIL-A-2550 APPLIES

2 MATERIAL: STEEL, CORROSION RESISTING, WIRE TYPE 303 CONDITION A OR B OR TYPE 416 CONDITION A PER ASTM A581.

3 FINISH: PASSIVATE PER 5.4.1 OF MIL-STD-171

4 SURFACE ROUGHNESS 125 ALL OVER

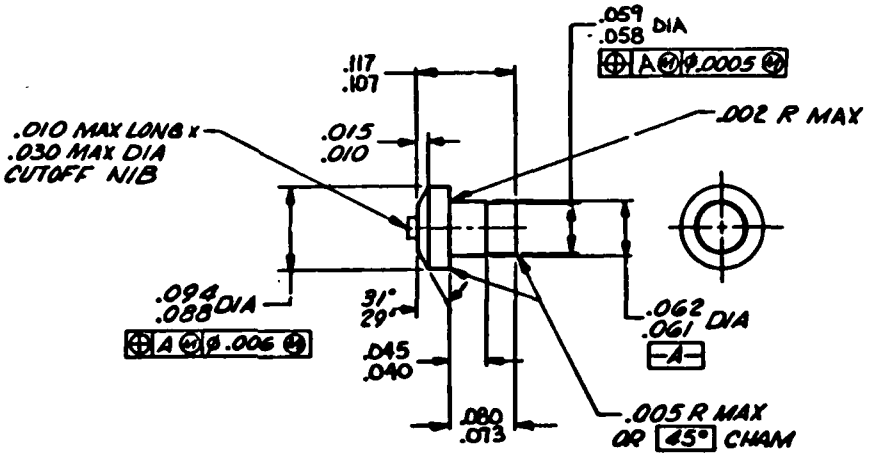

Figure B-4. Modifications for zigzag post.

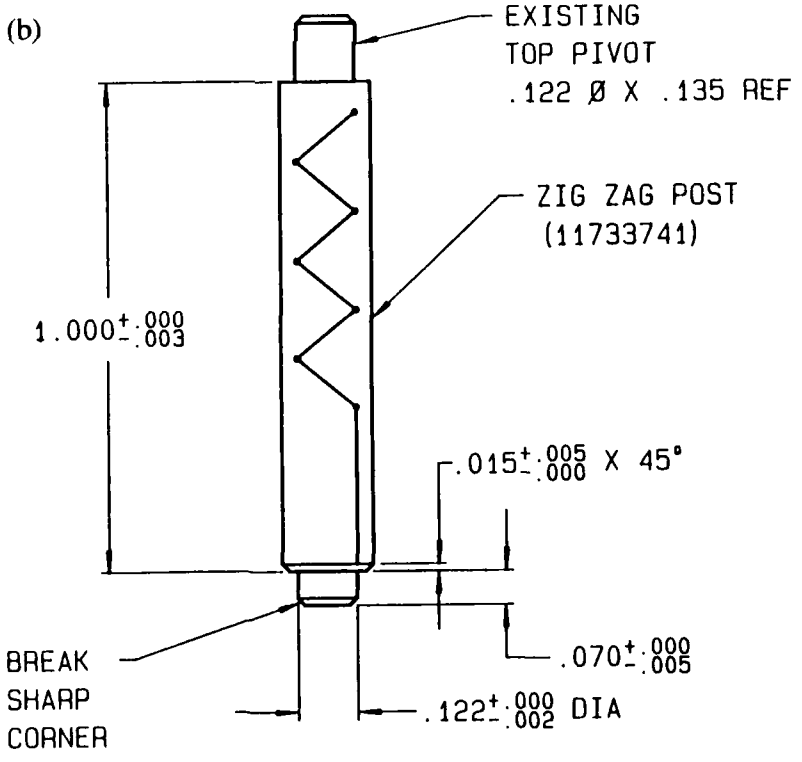

APPENDIX B

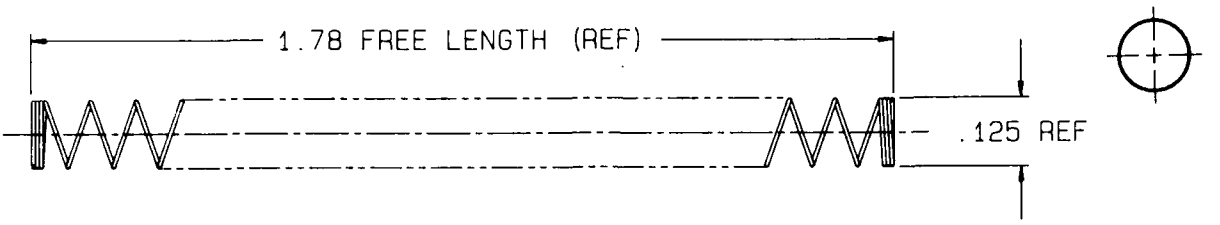

WIRE DIA. - .007
NO. OF ACTIVE COILS - 19
TOTAL NO. OF COILS - 25

NOTES:
1. MIL-A-2550 APPLIES.
2. MATERIAL: MUSIC WIRE.
3. DIRECTION OF HELIX: OPTIONAL.
4. MIN. I.D- .10
5. MAX. O.D- .13
6. FORCE AT HEIGHT OF .78 = 48 gm MIN
7. FORCE AT HEIGHT OF .38 = 68 gm MAX

Figure B-5. Bias spring.

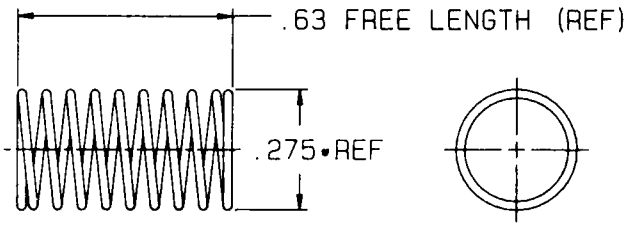

NOTES:
1. MIL-A-2550 APPLIES.
2. MATERIAL: MUSIC WIRE.
3. DIRECTION OF HELIX: OPTIONAL.
4. MIN. I.D-.20
5. MAX. O.D-.30
6. FORCE AT HEIGHT OF .40 = 35gm.
7. FORCE AT HEIGHT OF .30 = 50gm.

WIRE DIA.-.014
NO. COIL- 9
INSTALLED HEIGHT- .40
SPRING RATE= 150gm/in
STROKE= .1in

Figure B-6. Lock spring.

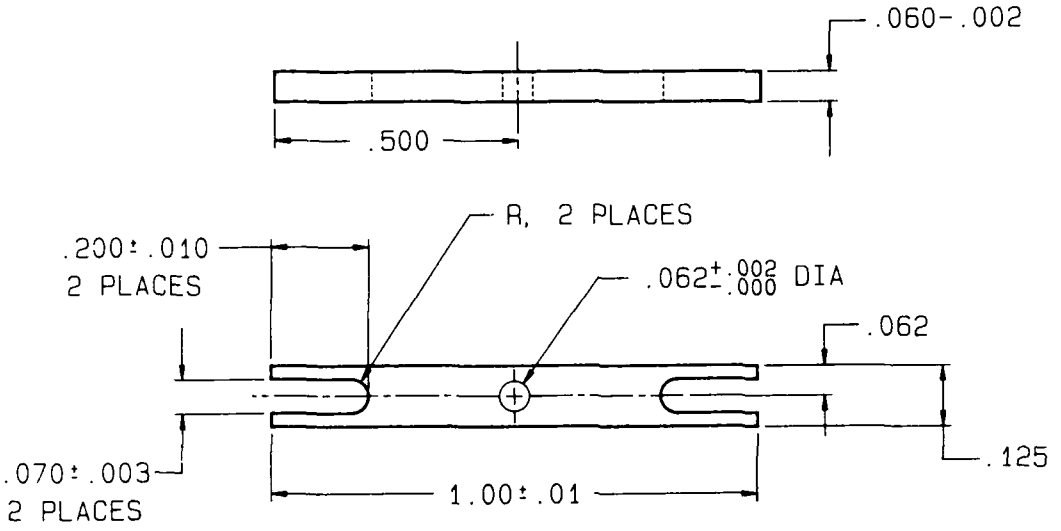

NOTES:
1. MIL-A-2550 APPLIES
2. MATERIAL ~ STAINLESS STEEL
3. 63 FINISH ALL OVER

Figure B-7. Actuator link.

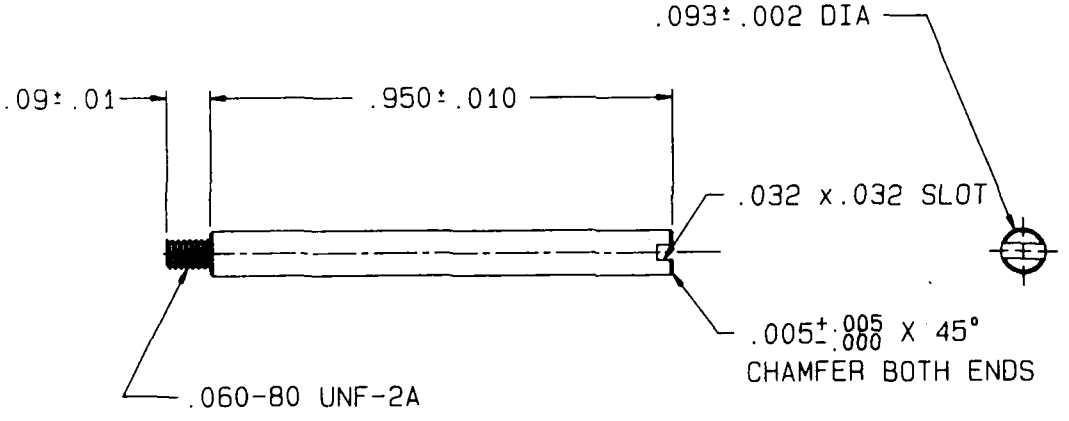

NOTES:
1. MIL-A-2550 APPLIES.
2. MATERIAL ~ STAINLESS STEEL.
3. 63 FINISH ALL OVER

Figure B-8. Guide rod.

APPENDIX B

Figure B-9. Solenoid modifications.

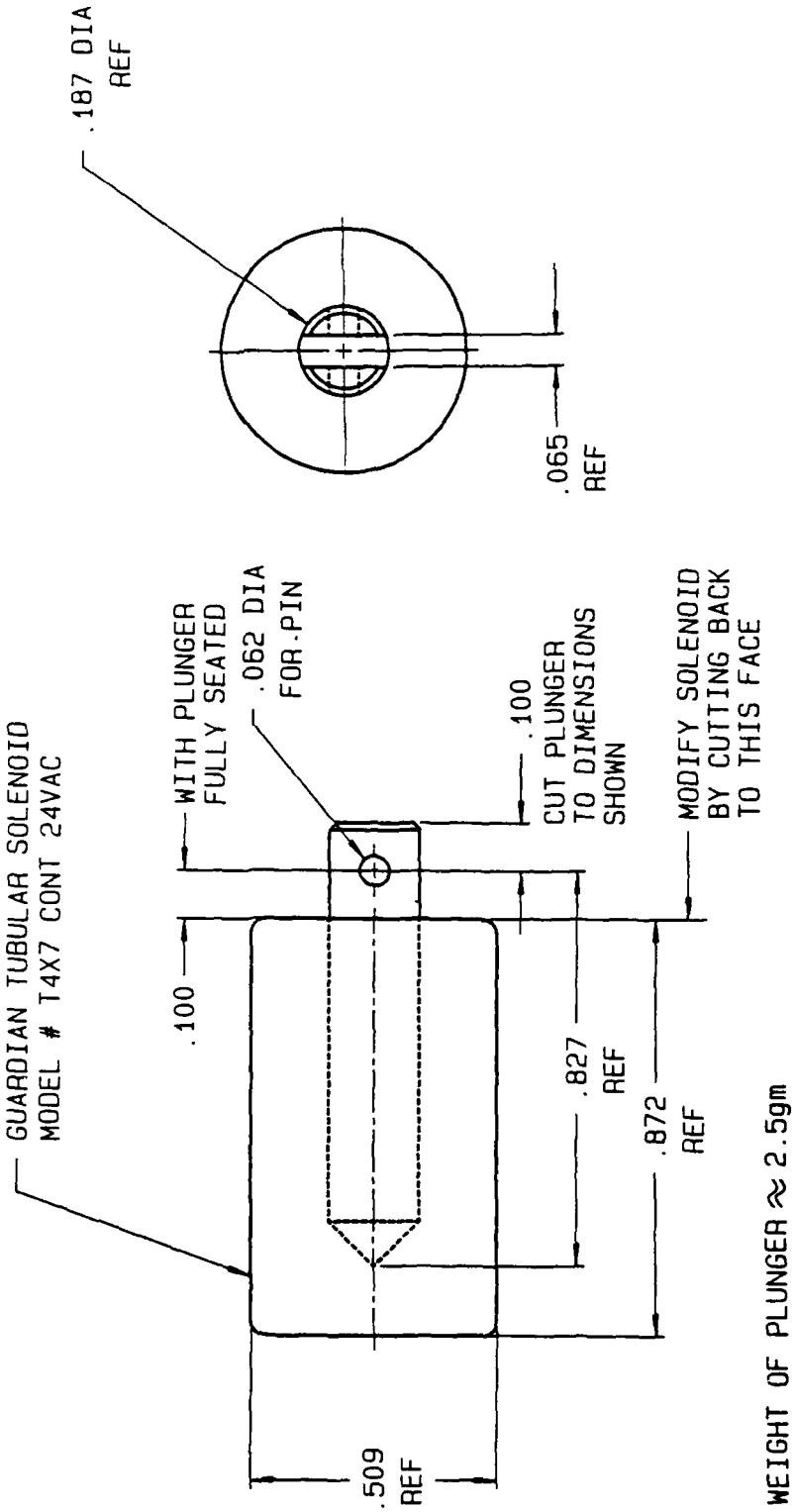

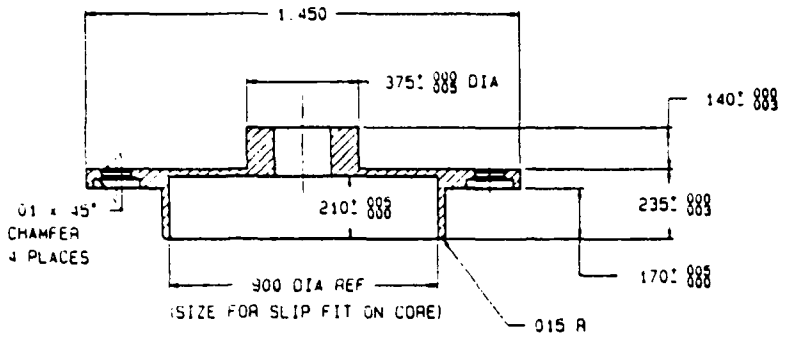

SECTION A-A

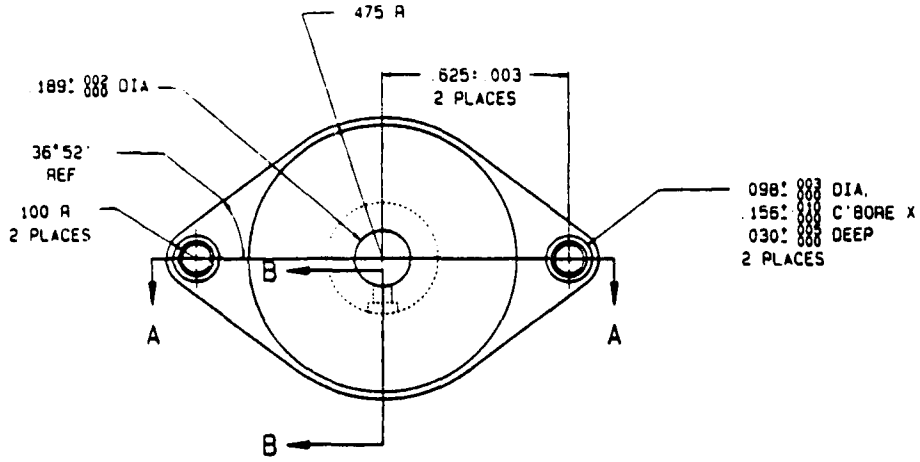

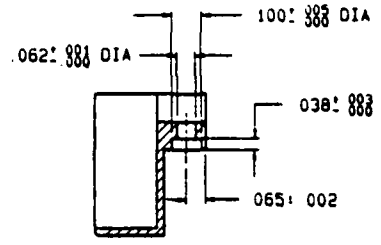

SECTION B-B

NOTES.
1. MIL-A-2550 APPLIES
2. MATERIAL ~ 303 STAINLESS STEEL
3. 63 FINISH ALL OVER

Figure B-10. Core holder.

APPENDIX B

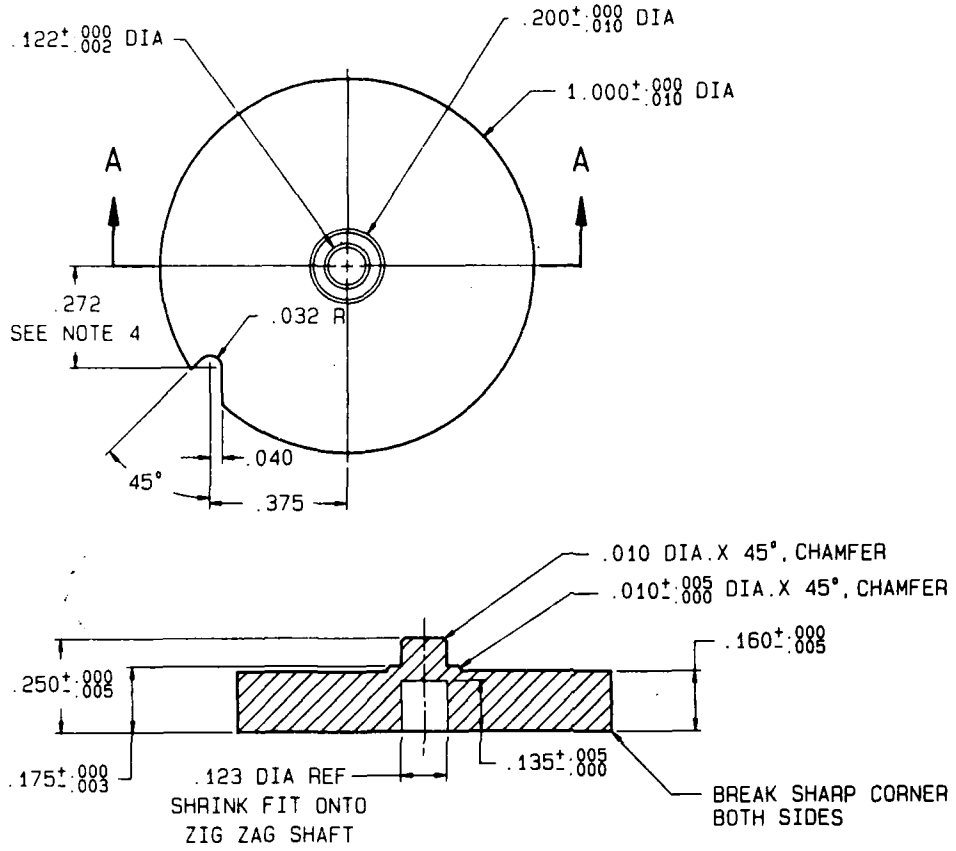

SECTION A-A

NOTES:
1. MIL-A-2550 APPLIES
2. MATERIAL ~ STAINLESS STEEL
3. 63 FINISH ALL OVER
4. LOCATE NOTCH AT FINAL ASSEMBLY. LOCATE 45° EDGE SUCH THAT PISTON DOES NOT BOTTOM OUT IN ACTUATOR HOUSING

Figure B-11. Flywheel.

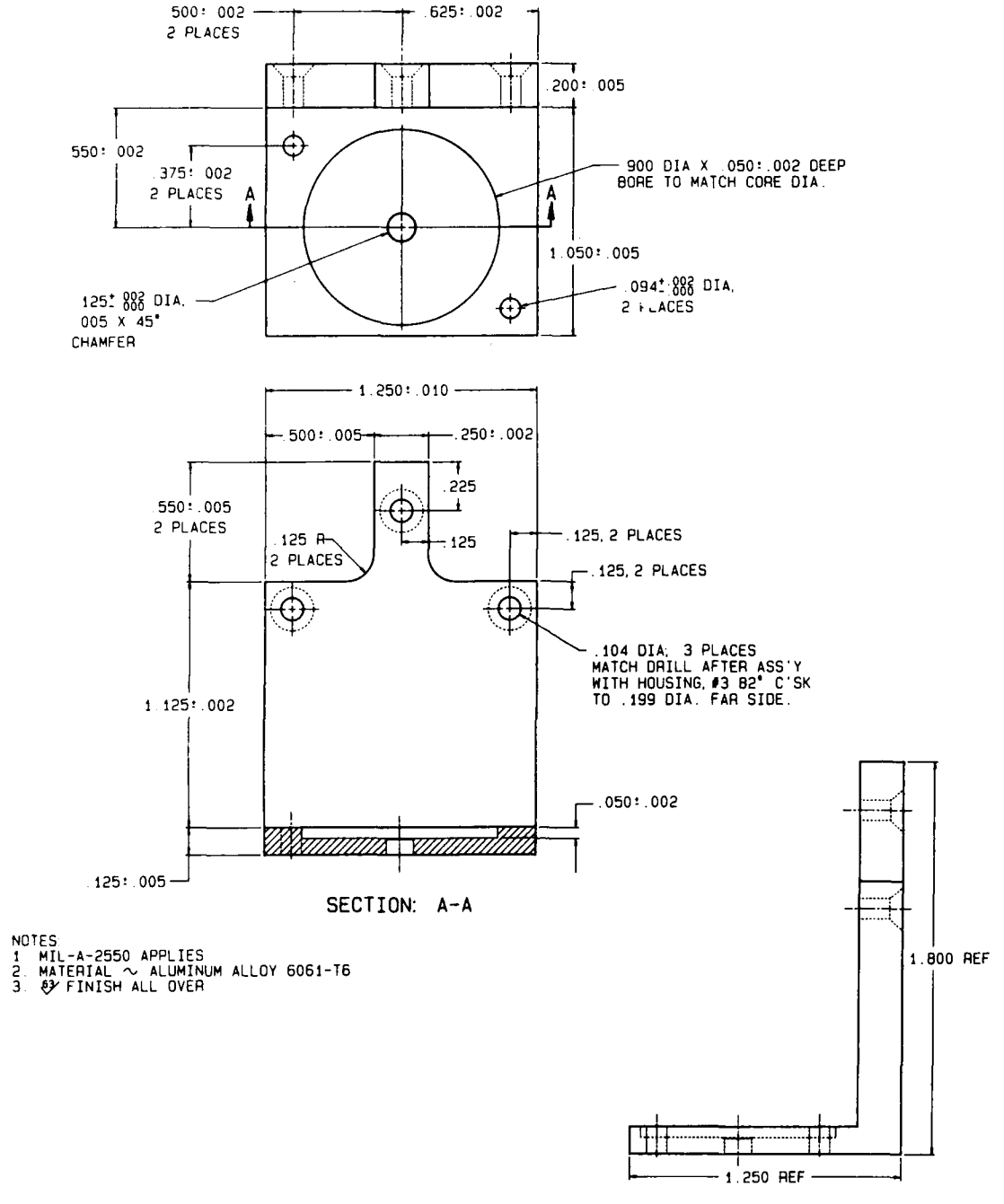

Figure B-12. Frame.

APPENDIX B

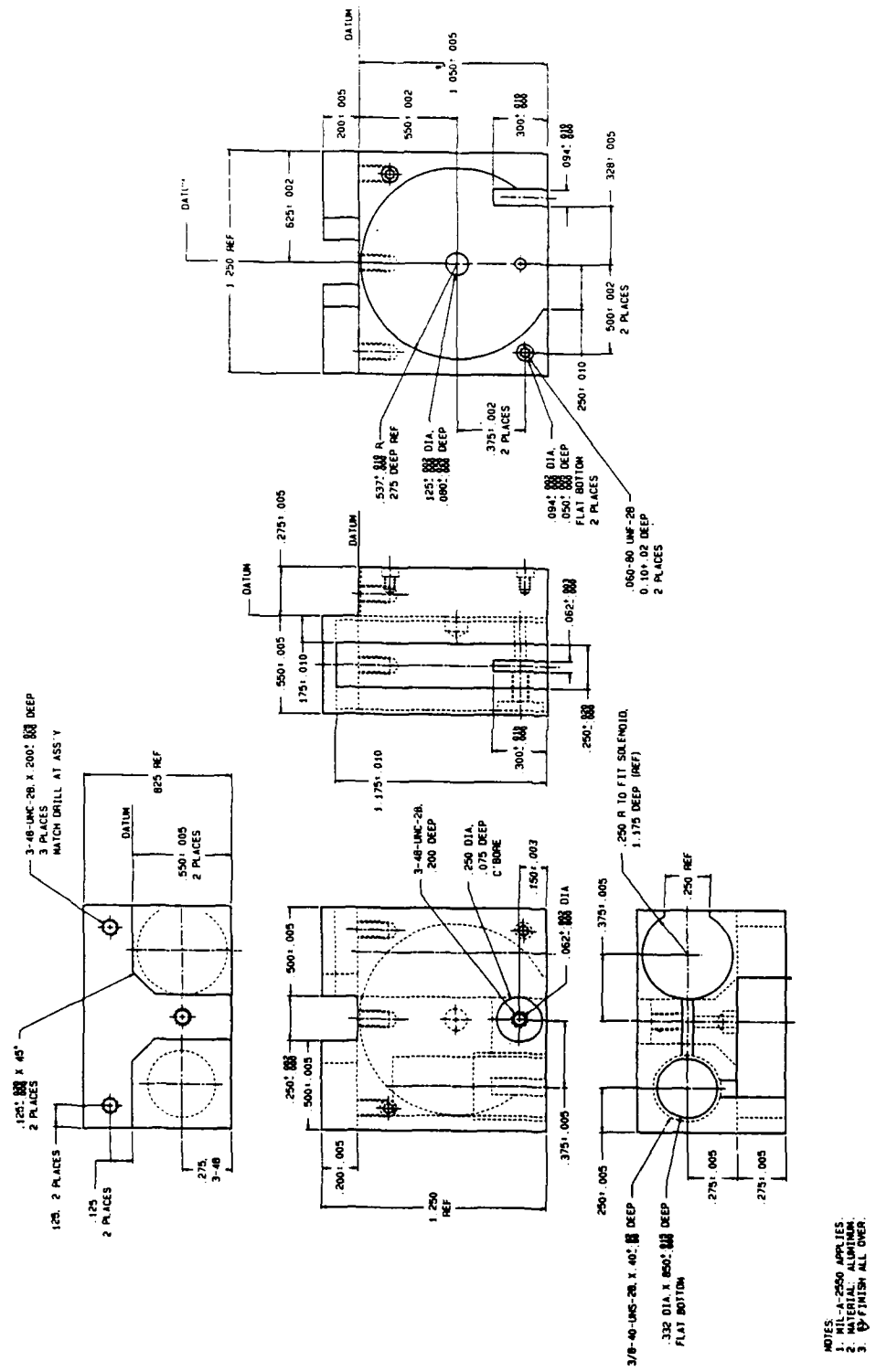

Figure B-13. Housing.

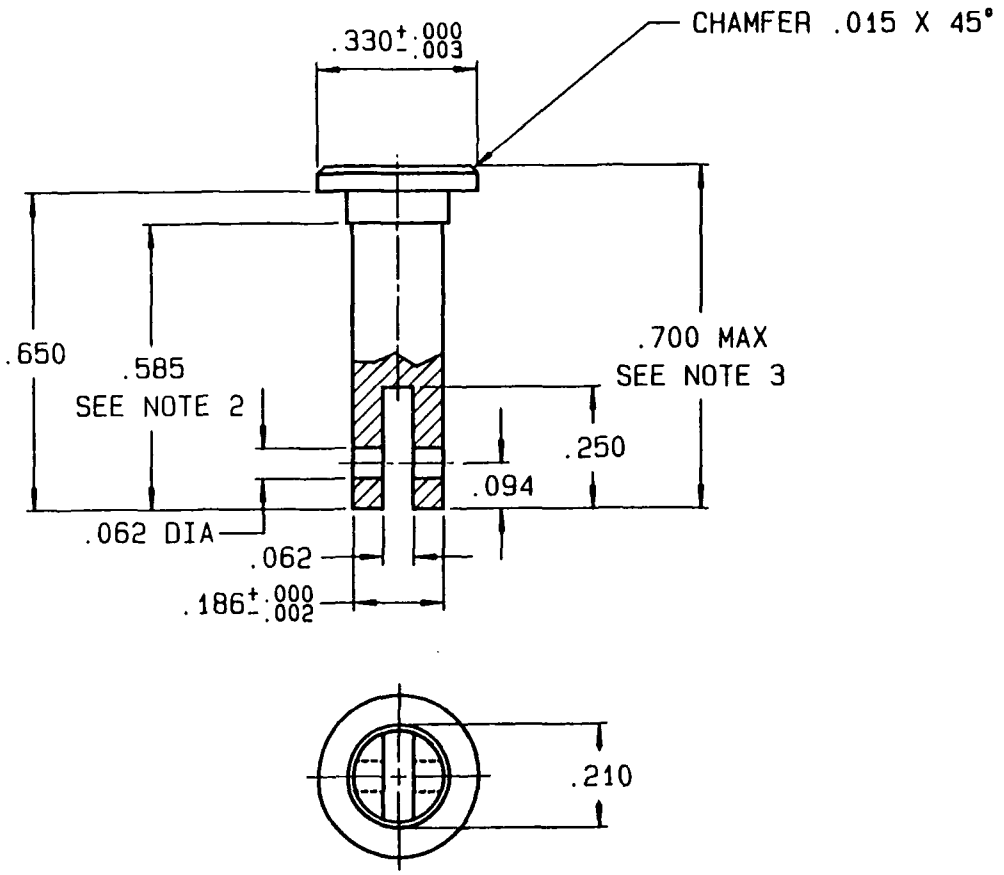

NOTES:
1. MATERIAL: STAINLESS STEEL
2. WEIGHT OF PISTON & PIN IS TO MATCH WEIGHT OF SOLENOID PLUNGER & LOCK PIN ASSEMBLY.
3. ADJUST LENGTH OF PISTON OR DEPTH OF HOLE IN HOUSING SUCH THAT PISTON DOES NOT BOTTOM-OUT IN THE HOLE IN BOTH THE FULL-SAFE AND FULL-ARMED POSITIONS.

Figure B-14. Piston.

APPENDIX B

Figure B-15. Retainer.

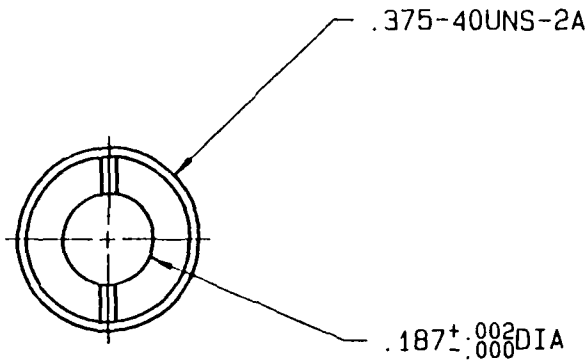

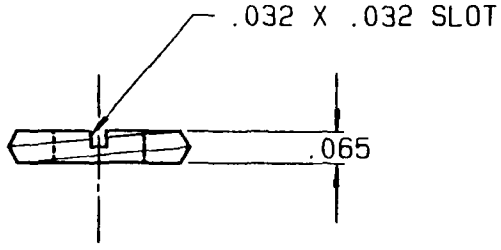

NOTE:
1. MATERIAL: BRASS

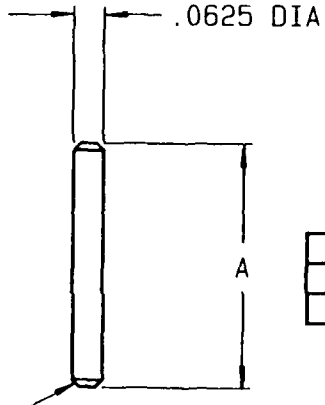

PART NO.	A DIM.
11730841-1	.40
11730841-2	.250

CHAMFER .015 X 45°
BOTH ENDS

NOTE:
1. MATERIAL: STAINLESS STEEL

Figure B-16. Pin, piston, and solenoid.

DISTRIBUTION

ADMINISTRATOR
DEFENSE TECHNICAL INFORMATION CENTER
ATTN DTIC-DDA (12 COPIES)
CAMERON STATION, BUILDING 5
ALEXANDRIA, VA 22304-6145

COMMANDER
US ARMY ARMAMENT, MUNITIONS, &
CHEMICAL COMMAND
ATTN SMCAR-LEP-L, TECHNICAL LIBRARY
ATTN SMCAR-ASF, FUZE & MUNITIONS
SUPPORT DIV
ATTN SMCAR-ESW-F, J. FAHL
ROCK ISLAND, IL 61299

DIRECTOR
US ARMY BALLISTIC RESEARCH LABORATORY
ATTN SLCBR-DD-T (STINFO)
ABERDEEN PROVING GROUND, MD 21005

US ARMY ELECTRONICS TECHNOLOGY
& DEVICES LABORATORY
ATTN SLCET-DD
FT MONMOUTH, NJ 07703

ENGINEERING SOCIETIES LIBRARY
ATTN ACQUISITIONS DEPARTMENT
345 EAST 47TH STREET
NEW YORK, NY 10017

DEPARTMENT OF ENERGY
ALBUQUERQUE OPERATIONS OFFICE
PO BOX 5400
ALBUQUERQUE, NM 87115

DIRECTOR
DEFENSE ADVANCED RESEARCH
PROJECTS AGENCY
ARCHITECT BLDG
ATTN WEAPONS TECH & CONCEPT DIV
1400 WILSON BLVD
ARLINGTON, VA 22209

DIRECTOR
DEFENSE INTELLIGENCE AGENCY
ATTN DT-2, WEAPONS & SYSTEMS DIV
WASHINGTON, DC 20301

UNDER SECRETARY OF DEFENSE
FOR RESEARCH & ENGINEERING
ATTN RESEARCH & ADVANCED TECH
WASHINGTON, DC 20301

OUSDR&E
ASSISTANT FOR RESEARCH
THE PENTAGON
WASHINGTON, DC 20301

ASSISTANT SECRETARY OF THE ARMY
RES, DEV, & ACQ
ATTN DEP FOR SCI & TECH
WASHINGTON, DC 20310

COMMANDER
US ARMY ARMAMENT, MUNITIONS, & CHEMICAL
COMMAND (AMCCOM)
US ARMY ARMAMENT RESEARCH &
DEVELOPMENT CENTER
ATTN SMCAR-FU, PROJECT MGT PROJECT OFC
ATTN SMCAR-CAWS, PM, CANNON ARTILLERY
WEAPONS SYSTEMS/SEMI-ACTIVE
LASER GUIDED PROJECTILES
ATTN SMCAR-AEF-C, S. HONICKMAN
ATTN SMCAR-AEF-C, F. TEPPER
ATTN SMCAR-AEF, L. HOROWITZ
ATTN SMCAR-AEF-C, E. BISSON
ATTN SMCAR-AEF, A NASH
ATTN AMCPM-FZ, T. SINCLAIR
ATTN AMCPM-FZ, J. MYDOSH
ATTN AMCPM-SA, PM, SELECTED AMMUNITION
ATTN SMCAR-TDR, RESEARCH & TECHNOLOGY
ATTN SMCAR-TDS, SYSTEMS DEV &
ENGINEERING
PICATINNY ARSENAL, NJ 07806-5000

DIRECTOR
BMD ADVANCED TECHNOLOGY CENTER
DEPARTMENT OF THE ARMY
PO BOX 1500
ATTN ATC-T
ATTN ATC-D
HUNTSVILLE, AL 35807

COMMANDING OFFICER
US ARMY FOREIGN SCIENCE
& TECHNOLOGY CENTER
FEDERAL OFFICE BLDG
ATTN AMXST-ES, ELECTRONICS SYS DIV
ATTN TECH LIBRARY
220 7TH STREET, NE
CHARLOTTESVILLE, VA 22901

COMMANDER
US ARMY MATERIEL COMMAND
ATTN AMCDE, DIR FOR DEVELOPMENT & ENG
5001 EISENHOWER AVE
ALEXANDRIA, VA 2233-0001

DIRECTOR
US ARMY MISSILE LABORATORY
USAMICOM
ATTN AMSMI-RPR, REDSTONE SCIENTIFIC
INFO CENTER
ATTN AMSMI-RPT, TECHNICAL
INFORMATION DIV

DIRECTOR
US ARMY MISSILE LABORATORY (cont'd)
USAMICOM
ATTN AMSMI-RN, CHIEF, TECHNOLOGY INTEGRATION OFFICE
ATTN AMSMI-RA, CHIEF, DARPA PROJECTS OFFICE
ATTN AMSMI-RR, RESEARCH DIR
ATTN AMSMI-RS, SYS ENGR DIR
ATTN AMSMI-RE, ADVANCED SENSORS DIR
ATTN AMSMI-RD-ST-WF, J. LIENAU
ATTN AMCPM-AM, C. SUPKO
ATTN AMSMI-ROC, W. ZECHER
ATTN AMCPO-HIP-HW, J. DUMBACHER
REDSTONE ARSENAL, AL 35809

COMMANDER
NAVAL SURFACE WEAPONS CENTER
ATTN DX-21 LIBRARY DIV
ATTN G30, M. SHAMBLEN
DAHLGREN, VA 22448-5180

COMMANDER
NAVAL SURFACE WEAPONS CENTER
ATTN E-43, TECHNICAL LIB
ATTN G44, G. KLAMM
ATTN G44, A. MUNACH
ATTN G44, R. NIEMEYER
ATTN G44, J. HORTON
ATTN G41, G. AMATO
ATTN U11, D. HINLEY
ATTN U24, G. GRAVETT
WHITE OAK, MD 20910

COMMANDER
NAVAL WEAPONS CENTER
ATTN TECH LIBRARY
ATTN 3353, R. PERRINE
ATTN 3353, S. ROHDE
ATTN 3353, J. McVAY
ATTN 335, R. HIGUERA
CHINA LAKE, CA 93555-6001

COMMANDER
AIR FORCE ARMAMENT & TEST LABORATORY
ATTN AFATL-MNF, R. MABRY
ATTN AFATL-MNF, D. FINELLO
ATTN AFATL-ADYN, E. SMITH
EGLIN AIR FORCE BASE, FL 32542-5000

DIRECTOR
NASA
GODDARD SPACE FLIGHT CENTER
ATTN 250, TECH INFO DIV
GREENBELT, MD 20771

ADVANCED TECH & RESEARCH
ATTN W. PICKLER
3933 SANDY SPRING RD
BURTONSVILLE, MD 20866

BREED CORP
ATTN T. THUEN
170 BEAVER BROOK RD
LINCOLN PARK, NJ 07035

BULOVA SYSTEMS & INST CORP
ATTN M. ENEMAN
PO BOX 189 GREEN ACRES RD W
VALLEY STREAM, NY 11582-0189

ELECTRONICS DEVELOPMENT COTP
ATTN R. N. JOHNSON
6905 G OAKLAND MILLS RD
COLUMBIA, MD 21045

HAMILTON TECHNOLOGY INC
ATTN J. JAMES
101 N QUEEN ST BOX 4787
LANCASTER, PA 17604-4787

HONEYWELL, INC
ATTN J. THALHEIMER
7900 WESTPARK DR, MS-410
McLEAN, VA 22102-4299

JET PROPULSION LABORATORY
CALIFORNIA INSTITUTE OF TECHNOLOGY
4800 OAK GROVE DRIVE
ATTN TECHNICAL LIBRARY
PASADENA, CA 91103

KDI PRECISION PRODUCTS
ATTN A. E. DILZ
ATTN G. KRAMER
3975 McMANN RD
CINCINNATI, OH 45245

LOS ALAMOS NATIONAL LABORATORY
ATTN M7, W. HEMSING
LOS ALAMOS, NM 87545

MAGNAVOX ELECTRONIC SYSTEMS CO
ATTN G. WEBB
ATTN R. GOFF
1313 PRODUCTION RD
FT WAYNE, IN 46808

MICRONICS INTERNATIONAL INC
PO BOX 450
3001 ENTERPRISE ST
BREA, CA 92621

DISTRIBUTION (cont'd)

MOTOROLA, INC
GOVT ELEC GROUP-TED
ATTN R-6203, L. FARACE
ATTN R-1211, A. MITTENDORF
8220 E. ROOSEVELT ST
SCOTTSDALE, AZ 85257

RAYMOND ENGINEERING INC
ATTN C. SALTZMAN
ATTN R. WOLSKI

RAYMOND ENGINEERING INC (cont'd)
ATTN J. JERABEK
217 SMITH ST
MIDDLETOWN, CT 06457-1739

QUANTIC INDUSTRIES
ATTN K. E. WILLIS
990 COMMERCIAL ST
SAN CARLOS, CA 94070-4017

SANDIA NATIONAL LABORATORIES
ATTN DIV 9127, B. CHILDERS
ATTN DIV 2514, A. MEDINA
ALBUQUERQUE, NM 87185

US ARMY LABORATORY COMMAND
ATTN TECHNICAL DIRECTOR, AMSLC-TD
ATTN J. SPELLMAN, AMSLC-TP-PL

INSTALLATION SUPPORT ACTIVITY
ATTN LEGAL OFFICE, SLCIS-CC

USAISC
ATTN RECORD COPY, ASNC-ADL-TS
ATTN TECHNICAL REPORTS BRANCH,
ASNC-ADL-TR (2 COPIES)

HARRY DIAMOND LABORATORIES
ATTN D/DIVISION DIRECTORS
ATTN LIBRARY, SLCIS-IM-TL (3 COPIES)
ATTN LIBRARY, SLCIS-IM-TL (WOODBRIDGE)
ATTN J. DAVID, SLCHD-TA-OW
ATTN P. INGERSOLL, SLCHD-TA-O
ATTN R. GOODMAN, SLCHD-TA-OS
ATTN N. DOCTOR, SLCHD-TA-OP
ATTN L. COX, SLCHD-PO-P
ATTN J. SATTLER, SLCHD-PO-P
ATTN P. JOHNSON, SLCHD-ST-A
ATTN C. CAMPAGNUOLO, SLCHD-TA-OP
ATTN R. GOTTRON, SLCHD-IT-R
ATTN H. LESSER, SLCHD-IT-EB
ATTN J. MINER, SLCHD-IT-RE
ATTN D. HUNTER, SLCHD-TA-OS
ATTN J. BEARD, SLCHD-TA-OM
ATTN B. MARY, SLCHD-TA-OM
ATTN G. LOHMANN, SLCHD-TA-OM
ATTN D. OVERMAN, SLCHD-DE-OM (10 COPIES)

END
DATED
FILM
8-88
DTIC